



## RESEARCH ARTICLE

10.1029/2019JF005156

## Key Points:

- A simple mechanistic model is developed to explore the formation of single-thread rivers in a broad range of unvegetated substrates
- Results show single-thread rivers may form in barren muddy banks, consistent with experiments, ancient deposits, and modern rivers
- The model offers a new framework to interpret the ancient record of single-thread rivers on Earth and Mars

## Supporting Information:

- Supporting Information S1

## Correspondence to:

M. G. A. Lapôtre,  
mlapotre@stanford.edu

## Citation:

Lapôtre, M. G. A., Ielpi, A., Lamb, M. P., Williams, R. M. E., & Knoll, A. H. (2019). Model for the formation of single-thread rivers in barren landscapes and implications for pre-Silurian and Martian fluvial deposits. *Journal of Geophysical Research: Earth Surface*, 124. <https://doi.org/10.1029/2019JF005156>

Received 13 MAY 2019

Accepted 4 SEP 2019

Accepted article online 1 OCT 2019

## Model for the Formation of Single-Thread Rivers in Barren Landscapes and Implications for Pre-Silurian and Martian Fluvial Deposits

Mathieu G. A. Lapôtre<sup>1,2</sup> , Alessandro Ielpi<sup>3</sup> , Michael P. Lamb<sup>4</sup> ,  
Rebecca M. E. Williams<sup>5</sup> , and Andrew H. Knoll<sup>1,6</sup>

<sup>1</sup>Department of Earth & Planetary Sciences, Harvard University, Cambridge, MA, USA, <sup>2</sup>Now at Department of Geological Sciences, Stanford University, Stanford, CA, USA, <sup>3</sup>Harquail School of Earth Sciences, Laurentian University, Sudbury, Ontario, Canada, <sup>4</sup>Division of Geological & Planetary Sciences, California Institute of Technology, Pasadena, CA, USA, <sup>5</sup>Planetary Science Institute, Tucson, AZ, USA, <sup>6</sup>Department of Organismic & Evolutionary Biology, Harvard University, Cambridge, MA, USA

**Abstract** Flume experiments and field observations show that bank vegetation promotes the formation of narrow and deep single-thread channels by strengthening riverbanks. Consistent with this idea, the pre-Silurian fluvial record generally consists of wide monotonous sand bodies often interpreted as deposits of shallow braided rivers, whereas single-thread rivers with muddy floodplains become more recognizable in Silurian and younger rocks. This shift in the architecture of fluvial deposits has been interpreted as reflecting the rise of single-thread rivers enabled by plant life. The deposits of some single-thread rivers, however, have been recognized in pre-Silurian rocks, and recent field studies have identified meandering rivers in modern unvegetated environments. Furthermore, single-thread-river deposits have been identified on Mars, where macroscopic plants most likely never evolved. Here we seek to understand the formation of those rarely recognized and poorly characterized single-thread rivers in unvegetated landscapes. Specifically, we quantitatively explore the hypothesis that cohesive muddy banks alone may enable the formation of single-thread rivers in the absence of plants. We combine open-channel hydraulics and a physics-based erosion model applicable to a variety of bank sediments to predict the formation of unvegetated single-thread rivers. Consistent with recent flume experiments and field observations, results indicate that single-thread rivers may form readily within muddy banks. Our model has direct implications for the quantification of riverbank strengthening by vegetation, understanding the hydraulic geometry of modern and ancient unvegetated rivers, interpreting pre-Silurian fluvial deposits, and unraveling the hydrologic and climate history of Mars.

**Plain Language Summary** Plants tend to strengthen riverbanks, favoring the formation of single-thread rivers (i.e., relatively deep flows within a single channel) over that of braided rivers (i.e., relatively shallow flows distributed among several interlaced channels). In parallel, geologists have observed a shift in the structure of river deposits coincident with the evolution of land plants, commonly interpreted as the signature of the rise of single-thread rivers, sparked by plant life. However, recent studies have identified single-thread-river deposits in both modern unvegetated environments and in rocks that predate the greening of the continents, and deposits of ancient single-thread rivers have also been identified on Mars, where large plants realistically never evolved. Thus, single-thread rivers can clearly form in vegetation-free environments; here we seek to understand how. Employing a conceptual model based on the mechanics of river flow and bank erosion, we show that sticky mud may strengthen riverbanks enough to resist erosion and prevent river braiding, suggesting that mud alone could have enabled the formation of single-thread rivers on ancient Earth and Mars. The model may help to quantify plant-driven riverbank strength, understand river geometry in barren landscapes, interpret ancient river deposits on Earth, and, possibly, decipher the climate history of Mars.

### 1. Introduction

#### 1.1. Single-Thread and Meandering Rivers

Single-thread alluvial rivers are relatively deep and narrow, straight to sinuous streams that carry water and sediments downslope within a single channel. Among single-thread rivers, meandering rivers feature

©2019. The Authors.

This is an open access article under the terms of the Creative Commons Attribution License, which permits use, distribution and reproduction in any medium, provided the original work is properly cited.

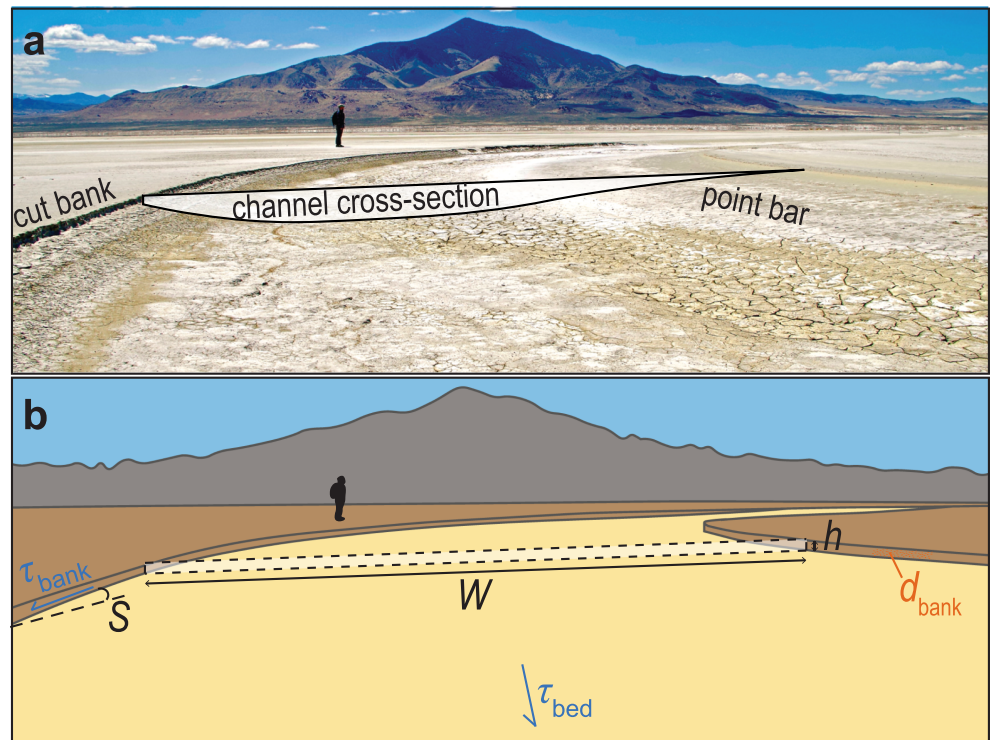


**Figure 1.** (a) Dry bed of a single-thread channel in unvegetated muddy banks (Bonneville Basin, UT, USA) and (b) definition sketch of main model parameters.

sinuous bends that grow in amplitude to the point of cutoff and maintain strikingly regular planform geometry across scales while snaking through low-lying floodplains (Leopold & Wolman, 1960; Williams, 1986). Meandering rivers migrate laterally at rates that generally increase with channel size and planform curvature (Braudrick et al., 2009; Hickin & Nanson, 1984; Howard & Knutson, 1984; Sylvester et al., 2019). Throughout this manuscript, we use “single-thread” as a sole descriptor of planform geometry; “meandering” is used for single-thread streams with bends that grow due to lateral migration.

In channel bends, flow inertia and scour lead to deeper flows along the outer bank (Bathurst et al., 1977). The resulting lateral pressure gradient leads to an in-channel helical flow that entrains sediment along the outer bank and transports it toward the inner bank further downstream, where it gets redeposited in the form of bank-attached bars (i.e., point bars; Figure 1a; Bluck, 1971; Jackson, 1975, 1976; Dietrich et al., 1979). To sustain meandering and to prevent the formation of midchannel bars, single-thread rivers require the formation of one main helical-flow cell across the width of a relatively narrow and deep channel. Thus, meandering rivers typically have low width-to-depth ratios (conservatively with  $W/h < \sim 200$  and often in the 20–100 range; Engelund & Skovgaard, 1973; Parker, 1976; McLelland et al., 1999; Gibling, 2006). Sinuous but non-meandering single-thread channels also have  $W/h < \sim 200$ , and straight single-thread rivers tend to form with even lower  $W/h$  (typically  $W/h < 10$ ; Parker, 1976). The  $W/h$  limit for river meandering (and thus single threads) arises from a midchannel bar instability that is well understood theoretically (e.g., Crosato & Mosselman, 2009; Seminara & Tubino, 1989; Struiksmas et al., 1985). Ultimately, because deeper flows impart greater shear stresses upon the riverbed and banks, the formation of single-thread rivers is intimately tied to the ability of riverbanks to resist erosion and confine relatively deep flows within a single relatively narrow channel (e.g., Ferguson, 1987; Schumm, 1960, 1963). Hence, natural single-thread alluvial streams tend to form in low-relief alluvial plains where bed stresses are buffered by gentle channel gradients (Ashmore, 1991; Smith & Smith, 1984) and where formative-discharge floods do not result in bank breach, channel branching, and eventual river braiding (Abdullatif, 1989; Bluck, 1974; Takagi et al., 2007).

Previous studies suggested that both higher mud contents in riverbanks (e.g., Schumm, 1960) and dense bank-vegetation covers (Graf, 1978; Huang & Nanson, 1998; Micheli & Kirchner, 2002; Murray & Paola, 2003; Smith, 1976) may slow bank erosion and lead to lower  $W/h$ . Even a thin cover of plants with shallow

roots seems to promote the formation of meandering rivers within otherwise cohesionless banks, perhaps through the armoring effect of vegetated slump blocks along the rivers' outer banks (e.g., Micheli et al., 2004; Parker et al., 2011). Untangling the effects of fine cohesive sediments and vegetation on natural rivers, however, is challenging. In addition to field studies and despite the difficulty of scaling bank erosion down to laboratory scales (e.g., Kleinhans et al., 2014; Kleinhans et al., 2015), some flume experiments have shown that either cohesive sediments (e.g., Peakall et al., 2007; van Dijk et al., 2012, 2013) or bank vegetation (e.g., Braudrick et al., 2009; Gran & Paola, 2001; Tal & Paola, 2007) can promote the formation of deeper and narrower, single-thread, and even meandering, channels. Given the ubiquity of plants in most terrestrial environments, bank vegetation likely provides a major control on the hydraulic geometry of modern rivers (e.g., Dietrich & Perron, 2006; Gurnell, 2014).

The relationship between bank vegetation and river planform geometry on modern Earth raises the question of what rivers might have looked like before the Silurian emergence of vascular plants (e.g., Cotter, 1978; de Almeida et al., 2016; Schumm, 1968). As a plant-devoid endmember, pre-Silurian river deposits may offer the opportunity to better constrain physical and biogeomorphic controls on river patterns. However, interpreting prevegetation fluvial deposits, and especially the planform geometry of rivers, is difficult. The sedimentary record of pre-Silurian fluvial systems generally displays monotonous and laterally extensive sand bodies (e.g., Davies & Gibling, 2010; Gibling, 2006; Gibling et al., 2014; Ielpi & Rainbird, 2016; Long, 1978, 2011), with the mud content of alluvial successions sharply increasing near the Ordovician-Silurian boundary (McMahon & Davies, 2018a). In turn, preserved heterolithic lateral accretion sets, characteristic of some meandering rivers, only become common in outcrop-scale exposures near the Silurian-Devonian boundary (e.g., Cotter, 1978; Davies et al., 2011; Davies & Gibling, 2010; Gibling et al., 2014). Altogether, the clear spatial and temporal relationship between single-thread rivers and vegetation in both modern and ancient environments supports the hypothesis that land-plant evolution has influenced the development of fluvial systems through time and that bank-strengthening vegetation promotes the formation of single-thread rivers.

It remains unclear, however, whether the interpreted paucity of pre-Silurian single-thread rivers reflects a true scarcity of such rivers before the advent of land plants, a lack of refined facies models applicable to non-heterolithic meandering systems (Hartley et al., 2015, 2018), or selective preservation of sandier deposits in the absence of vegetation. There is also a possibility that some Precambrian fluvial mudstones were misinterpreted as marine in the absence of fossils (McMahon & Davies, 2018a). Despite being rarely recognized (e.g., Gibling et al., 2014; Hartley et al., 2018; McMahon & Davies, 2018b), at least some single-thread rivers existed long before plants colonized land (Long, 1978, 2011; Ielpi & Rainbird, 2015; Santos & Owen, 2016; Ielpi et al., 2016, 2017). Moreover, some single-thread rivers meander on Earth today in the virtual absence of macroscopic plant life (Matsubara et al., 2015; Ielpi, 2018; Ielpi & Lapôtre, 2019a-b; Santos et al., 2019). Finally, another barren endmember of single-thread rivers comes from Mars. Although its surface is largely cold and dry today, abundant evidence suggests that Mars once had an active surface hydrological cycle, with lakes, rivers, and deltas (Di Achille & Hynes, 2010; Fassett & Head, 2008; McLennan et al., 2019). In particular, many sinuous ridges on Mars are thought to be remnants of deposits from sinuous-to-meandering rivers where neighboring floodplain deposits have been deflated and channel fills or channel-belt deposits now stand in positive relief (Burr et al., 2010; Cardenas et al., 2018; DiBiase et al., 2013; Kite et al., 2015; Williams et al., 2013). It is thus clear that, even though land plants play a significant role in shaping single-thread streams on Earth today, they are not a necessary condition for single-thread rivers to form.

If bank strength is necessary to form single-thread rivers, strengthening agents other than plants must have played a role on the pre-Silurian Earth and ancient Mars; candidates include ground ice, cements, and cohesive mud. Even though single-thread rivers are found in terrestrial permafrost, they often have vegetated banks (e.g., Matsubara et al., 2015). Furthermore, ice has been shown to promote bank erosion where temperatures oscillate annually around the freezing point of water (Hinkel & Hurd, 2006; Lawler, 1986; Scott, 1978; Wolman, 1959), a necessary condition for liquid water to be stable within the channel while ground ice permeates riverbanks. Altogether, any relationship between ground ice and single-thread rivers remains unclear. Salts, carbonates, and phyllosilicates are abundant on Earth, have been detected by spectrometers orbiting Mars (e.g., Ehlmann et al., 2008; Ehlmann & Edwards, 2014; Mustard et al., 2008; Poulet et al., 2005), and may have provided cohesion to ancient terrestrial and Martian riverbanks. However, cementing chemical precipitates may dissolve by contact of flowing unsaturated water. The few terrestrial unvegetated

rivers that are single threaded (and even meander) occur in mud-prone endorheic basins (e.g., Figure 1a; Matsubara et al., 2015; Ielpi, 2018; Ielpi & Lapôtre, 2019a, 2019b), leaving mud as the simplest explanation for the formation of single-thread rivers on ancient Earth and Mars.

Part of the issue in evaluating the importance of different bank strengthening mechanisms is that, even though sophisticated theoretical and numerical models have been developed to study the formation and dynamics of single-thread and meandering rivers (e.g., Crosato & Saleh, 2011; Eaton et al., 2004; Eaton et al., 2006; Howard & Knutson, 1984; Ikeda et al., 1981; Limaye & Lamb, 2013; Matsubara & Howard, 2014; Millar, 2000; Millar & Quick, 1993, 1998; Parker, 1976; Parker et al., 2011), few studies have attempted to relate bank strength quantitatively to channel planform (Dunne & Jerolmack, 2018). Even studies that have attempted to relate river planform to bank properties parameterized bank strength through a single parameter that encompasses all physical, chemical, and biological contributions and requires field calibration for individual rivers (Eaton et al., 2004; Millar, 2000; Millar & Quick, 1993, 1998). Specifically, there is no physics-based model capable of predicting the formation of single-thread rivers within a wide range of riverbank materials and that does not systematically require field calibration of bank erodibility. To bridge this gap, we develop a theory for the formation of single-thread rivers in barren landscapes and evaluate it against observations of ancient fluvial deposits on Earth and Mars.

## 1.2. Goals

The overarching goal of this study is not to capture the complex dynamics of single-thread rivers but, rather, (i) to provide a first-order mechanistic model for the capacity of mud to confine water within a single channel (section 3) and (ii) to develop a new quantitative method to interpret the deposits of unvegetated rivers (section 4). We focus on mud (clays + silt) because it is ubiquitous on Earth today, in ancient (including pre-Silurian) sedimentary rocks (e.g., Tosca et al., 2010) and in ancient Martian terrains (e.g., Ehlmann & Edwards, 2014), and may be the primary bank-strengthening agent that allows for single-thread rivers in many environments (Dunne & Jerolmack, 2019). Determining whether mud alone can cause the formation of single-thread rivers is important because field observations of single-thread rivers in mud-prone environments is often confounded by the presence of cementing sulfates and putative biofilms on Earth (e.g., Ielpi, 2018) and because properly scaling flume experiments is challenging (e.g., Kleinhans et al., 2014; 2015). Building on our model results, we discuss implications for quantifying the effect of vegetation on bank strength (section 4.1), the hydraulics of modern unvegetated single-thread rivers (section 4.2), paleohydraulic applications to pre-Silurian fluvial sedimentary rocks (section 4.3), and hydrologic and climate scenarios for Early Mars (section 4.4).

## 2. Model: Single-Thread Rivers Without Plants

We develop a simple model to relate a river's equilibrium width-to-depth ratio ( $W/h$ ) to a set of quantities that are readily measurable in the field and then use  $W/h$  as a proxy for river planform geometry (Engelund & Skovgaard, 1973; Parker, 1976). Channel width is often difficult to quantify in the sedimentary record, given the rare occurrence of outcrops that are laterally continuous over the 100- to 1,000-m scale of most natural channels (Ghinassi et al., 2013) and a general lack of preserved stratal features that can be interpreted in terms of channel width (e.g., channel fills). In contrast, channel depth may readily be estimated from bedforms, bar cross set thicknesses (e.g., Bradley & Venditti, 2019; Mohrig et al., 2000), and channel-belt thicknesses (Hayden et al., 2019). In the following, we thus use flow depth,  $h$ , as a known input parameter to estimate  $W$ , although the model could easily be formulated to use  $W$  as an input and to output  $h$ .

### 2.1. Channel Equilibrium Width

The width of rivers in cohesionless substrates attain equilibrium when net bank erosion is null (e.g., Métivier et al., 2017; Parker, 1978). Similarly, the equilibrium width of alluvial rivers forming within cohesive banks must be such that, on average, net bank erosion is null (e.g., Millar & Quick, 1993, 1998; Millar, 2000; Dunne & Jerolmack, 2019). Whereas such an equilibrium can either be static (and achieved through the total absence of erosion and deposition) or dynamic (and be achieved through any given amount of bank erosion being compensated by the same amount of deposition), either scenario requires the mean depth-averaged

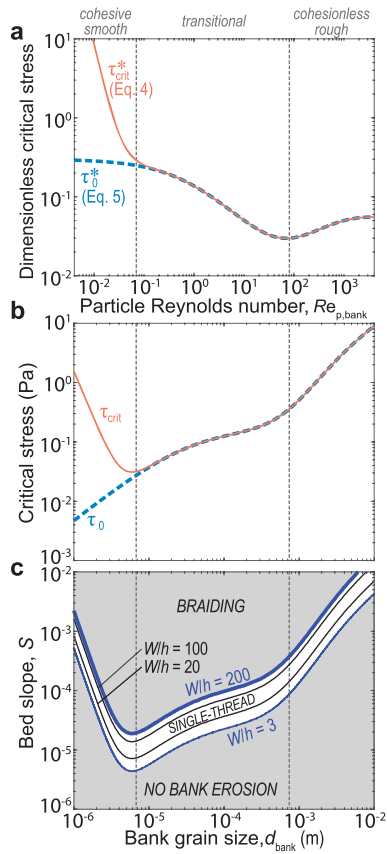


**Figure 2.** (a) Dimensionless critical stress for erosion as a function of bank-specific particle Reynolds number, (b) critical shear stresses for erosion as a function of  $d_{\text{bank}}$ , and (c) predicted  $W/h$  as a function of  $d_{\text{bank}}$  and  $S$  (calculated with Earth-like parameters; Table 1). In (c), the predicted stability field of single-thread rivers is left unshaded.

bank stress ( $\tau_{\text{bank}}$ ), as averaged over both inner and outer banks, to be close to the threshold for the erosion of bank materials ( $\tau_{\text{crit}}$ ; Dunne & Jerolmack, 2018), that is,

$$\tau_{\text{bank}} \approx \tau_{\text{crit}}. \quad (1)$$

## 2.2. Bank Stresses

Shear stresses exerted by water on the banks is a function of bed shear stress and channel cross-sectional shape (e.g., Flinham & Carling, 1988; Kean et al., 2009; Kean & Smith, 2004; Knight et al., 1984; Nelson & Seminara, 2011) and may be estimated through

$$\tau_{\text{bank}} = \varepsilon \tau_{\text{bed}}, \quad (2)$$

where  $\varepsilon$  is a stress-partitioning function and where total bed shear stress ( $\tau_{\text{bed}}$ ; skin friction + form drag) can be estimated from bed slope ( $S$ ) and  $h$  assuming steady, uniform flow conditions ( $\tau_{\text{bank}} = \tau_{\text{bed}} = \rho g h S$ , with  $\rho$  the density of water and  $g$  the acceleration of gravity) for modern rivers, or from sedimentological constraints of bed regime for ancient deposits (e.g., Lapôtre et al., 2017). We employ the stress-partitioning function of Knight et al. (1984) and Flinham and Carling (1988) for a rectangular channel, assuming similar wall and bed roughness (Text S1),

$$\varepsilon = \frac{1.77 \frac{W}{2h}}{\left(\frac{W}{2h} + \frac{3}{2}\right)^2 - 1.77}. \quad (3)$$

Intuitively, stresses partition such that  $\tau_{\text{bank}} \sim \tau_{\text{bed}}$  for narrow and deep channels ( $W/h \sim 1$ ) and  $\tau_{\text{bank}} \rightarrow 0$  in the limit of very wide and shallow rivers ( $W/h \rightarrow \infty$ ). Even though  $\varepsilon$  was determined empirically, it is defined as the ratio of two shear stresses that have the same gravity dependence, such that it should be applicable to the Martian environment.

## 2.3. Critical Stress for Bank Erosion

The critical stress for bank erosion is a complex function of bank materials and fluid properties (Grabowski et al., 2011). Perhaps owing to this complexity, bank strength has most often been taken into account through a single parameter—an effective bank friction angle (e.g., Eaton et al., 2004; Millar, 2000; Millar & Quick, 1993, 1998) that encompasses all strengthening effects (e.g., grain contacts, mud cohesion, and vegetation). Rather than parameterizing bank resistance to erosion through a single parameter, here we explicitly model the effect of cohesive sediments on the bank erosion threshold,  $\tau_{\text{crit}}$ . We utilize the model of Ternat et al. (2008) to predict  $\tau_{\text{crit}}$  as a function of grain size within the banks ( $d_{\text{bank}}$ ).

Ternat et al. (2008) assume that cohesion arises for fine clay-to-silt-sized particles through van der Waals forces and neglects structural and double-layer electrostatic interactions. These assumptions are most valid for water-saturated materials that are not fully consolidated, as is expected in the active surface layer of riverbanks (see also Text S2). Whereas banks are modeled with a single effective grain size to limit the number of variables in this analysis, the model formulation has the capability to determine cohesion for a mixture of different grain sizes (Ternat et al., 2008). In dimensionless form,

$$\tau_{\text{crit}}^* = \frac{\tau_{\text{crit}}}{(\rho_s - \rho) g d_{\text{bank}}} = \tau_0^* \left(1 + \frac{F_c}{F_w}\right), \quad (4)$$

where  $\rho_s$  is sediment density,  $\tau_0^*$  is the critical Shields stress for the incipient motion of loose sediment, and  $F_c$  and  $F_w$  are the cohesive force and weight of particles, respectively. For relatively large particles, the critical stress for erosion is determined by the Shields stress for cohesionless sediment, whereas for small particles, the cohesive-force term dominates, and the critical stress for bank erosion becomes significantly greater than

that for cohesionless particles (Figures 2a and 2b). The fit of Soulsby and Whitehouse (1997) to experimental data for the Shields stress of cohesionless grains is used,

$$\tau_0^* = \frac{0.3}{1 + 1.2\text{Re}_{p,\text{bank}}^{2/3}} + 0.055 \left[ 1 - \exp\left(-0.02\text{Re}_{p,\text{bank}}^{2/3}\right) \right], \quad (5)$$

where  $\text{Re}_{p,\text{bank}} = \frac{(Rgd_{\text{bank}}^3)^{1/2}}{\nu}$  is a bank-specific particle Reynolds number, with  $R = \frac{\rho_s - \rho}{\rho}$  being the submerged specific density of sediment, and  $\nu$  is kinematic viscosity of the fluid (Text S2).

Particle weight is given by

$$F_w = k_w(\rho_s - \rho)gd_{\text{bank}}^3, \quad (6)$$

where  $k_w$  is a shape factor equal to  $\pi/6$  for spherical particles. Under the assumption of a single grain size (Text S2), the cohesive force is calculated through

$$F_c = A_h \beta \frac{(1 - \cos\phi)}{48K_n^2 d_{\text{bank}}}, \quad (7)$$

where  $A_h \approx 10^{-20}$  is the Hamaker constant,  $\beta$  is the coordination number of sediment grains,  $\phi$  is a characteristic angle of internal friction, and  $K_n$  is the compaction function given by

$$K_n = \left( \frac{n_{\text{max}} - n_c}{n_{\text{max}} - n} \right)^{1/3} - 1, \quad (8)$$

with  $n$  the porosity and  $n_c$  and  $n_{\text{max}}$  are the fully compacted and maximum porosities, respectively (Ternat et al., 2008). Ternat et al. (2008) do not define  $\phi$  as a friction angle in the Mohr-Coulomb sense (i.e.,  $\tan\phi \neq \frac{\tau - c}{\sigma_n}$  where  $\tau$  and  $\sigma_n$  are the shear and normal stresses, respectively, and cohesion,  $c$ , is accounted for in the numerator) but rather as the ratio of driving to stabilizing forces (i.e.,  $\tan\phi = \frac{F_d}{F_w - F_l + F_c}$  where  $F_d$  and  $F_l$  are drag and lift forces, respectively, and where the cohesive force,  $F_c$ , is accounted for in the denominator); hence, it has a higher value than those typically reported for granular materials in geotechnical studies. Rewriting  $\tau_{\text{crit}}^*$  as a function of  $\text{Re}_{p,\text{bank}}$  using equations (4)–(8), we express the model of Ternat et al. (2008) as

$$\tau_{\text{crit}}^* = \tau_0^*(\text{Re}_{p,\text{bank}}) \left[ 1 + \Omega \text{Re}_{p,\text{bank}}^{-2} \right], \quad (9)$$

where  $\Omega = \frac{A_h \beta (1 - \cos\phi)}{48K_n^2 k_w \rho \nu^2 d_{\text{bank}}}$  is a dimensionless number describing the ratio of energies associated with van der Waals interactions (and thus a function of sediment compaction through  $\beta$  and  $K_n$ ) and grain-scale viscous energy. Assuming hexagonal close packing of sediment grains, we set  $\beta = 12$  and  $n_c = 1 - \frac{\pi}{3\sqrt{2}} \approx 0.26$ , and following Ternat et al. (2008), we set  $\phi = 52.5^\circ$  and  $n_{\text{max}} = 1$ . These values yield accurate results for natural granular materials (Ternat et al., 2008).

#### 2.4. Cohesion of Vegetated Banks

Previous studies have quantified the effect of vegetation on bank strength for specific rivers or particular plant species (e.g., Micheli et al., 2004; Micheli & Kirchner, 2002; Polvi et al., 2014; Simon & Collison, 2002). Here we take a simpler, more general approach and include vegetation into equation (4) with a single parameter,

$$\tau_{\text{crit},\text{total}}^* = \tau_{\text{crit}}^* + \tau_{\text{veg}}^* = (1 + \sigma^*) \tau_0^* \left( 1 + \frac{F_c}{F_w} \right), \quad (10)$$

where  $\sigma^*$  is a dimensionless strength factor describing vegetation-added strength and is defined as  $\sigma^* = \frac{\tau_{\text{veg}}^*}{\tau_{\text{crit}}^*}$  with  $\tau_{\text{veg}}^* = \frac{\tau_{\text{veg}}}{(\rho_s - \rho)gd_{\text{bank}}}$  and  $\tau_{\text{veg}}$  being the additional fluid stress to erode banks required by the presence of

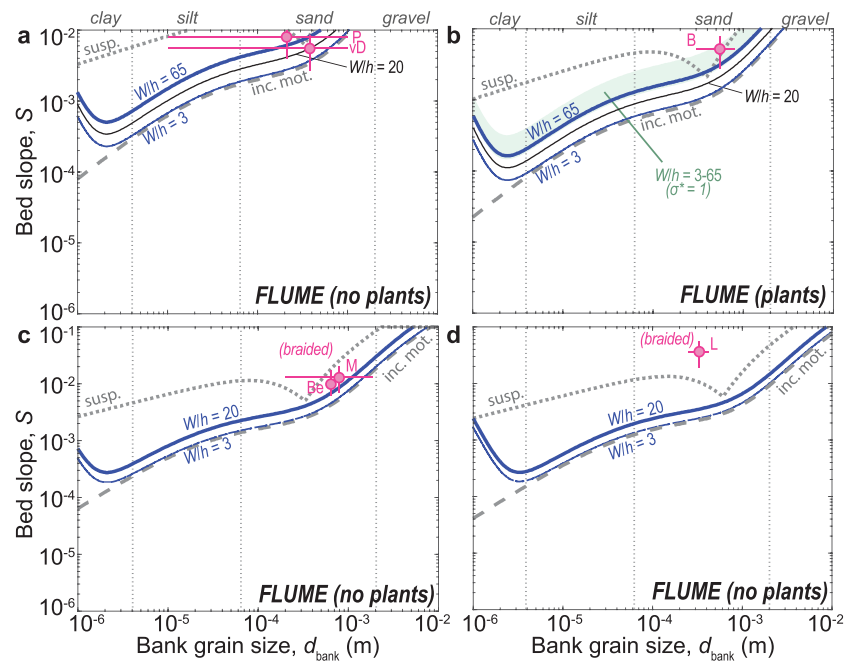


**Figure 3.** Predicted  $W/h$  for laboratory-scale experimental rivers using input parameters representative of the experiments of (a) Peakall et al. (2007; P) and van Dijk et al. (2012; vD), (b) Braudrick et al. (2009; B), (c) Moreton et al. (2002; M) and Bertoldi et al. (2009; Be), and (d) Limaye et al. (2018; L). Table 1 summarizes model input parameters for each panel and Table 2 those used in the experiments. To take into account the dependence of the threshold  $W/h$  with  $S$ , the approximate stability field for single-thread rivers is indicated by contours of  $W/h$  between 3 and 65 for predictions compared to experiments with shallower slopes (a,b;  $S \sim 10^{-3} - 10^{-2}$ ) and 20 for those compared to experiments with steeper slopes (c,d;  $S \sim 10^{-2} - 10^{-1}$ ). The thresholds of motion (gray dashed lines; Soulsby & Whitehouse, 1997) and of suspension (gray dotted lines; Niño et al., 2003) are added for comparison. In (b), the shaded green area highlights the  $W/h = 3-65$  contours for  $\sigma^* = 1$ .

vegetation. We do not know the functional form of  $\tau_{veg}^*$ , so we use equation (10) only to determine the value of  $\sigma^*$  that minimizes the discrepancy between data from vegetated rivers and model predictions.

### 2.5. Formation of Single-Thread Channels

By substituting equations (2) and (4) into equation (1), we solve for river equilibrium width ( $W$ ) and  $W/h$  as a function of eight main input variables— $h$ ,  $S$  (or shear velocity,  $u_* = \sqrt{\tau_{bed}/\rho}$ ),  $d_{bank}$ ,  $g$ ,  $\rho$ ,  $\rho_s$ ,  $\nu$ , and  $n$  (we keep all other parameters constant). Our approach is similar to that of Millar and Quick (1993, 1998), Millar (2000), and Eaton et al. (2004) but with two main differences: (i) Bank cohesion in our model is calculated as a function of grain size and other properties of bank sediments using an explicit first-principle model, and (ii) the model does not require an optimization condition on bed slope, sediment transport, or flow resistance because channels are assumed to be rectangular (Bui et al., 2000).

Parker (1976) showed that  $W^*$ , the maximum  $W/h$  achieved by single-thread rivers at the meandering-to-braiding transition, depends on bed slope (i.e.,  $W^* = \frac{Fr}{S} = \frac{1}{\sqrt{C_f S}}$  under steady uniform flow conditions, where  $Fr$  is the flow Froude number and  $C_f$  is a dimensionless friction coefficient) but not on gravity (at least to first order; gravity may affect, e.g., bedforms, and thus  $C_f$ ). According to Parker (1976), rivers develop midchannel bars and braid at  $W^* \approx 100 - 200$  (Text S3). Given the dependence of  $W^*$  on channel slope and to account for the wide range in bed slope spanned by the natural and experimental rivers we next investigate, we use three different  $W^*$  values that follow a  $W^* \propto \frac{1}{\sqrt{S}}$  dependence. We employ a conservative value of  $W^* = 200$  to illustrate the braiding-to-single-thread transition for  $S < 10^{-3}$ ,  $W^* = 65$  for  $S \sim 10^{-3} - 10^{-2}$ , and  $W^* = 20$  for  $S \sim 10^{-2} - 10^{-1}$ . Because  $W^*$  is not expected to vary significantly with gravity, we use the same  $W^*$  values for Earth and Mars. The stress-partitioning model we use only applies to single-thread rivers; thus, while our

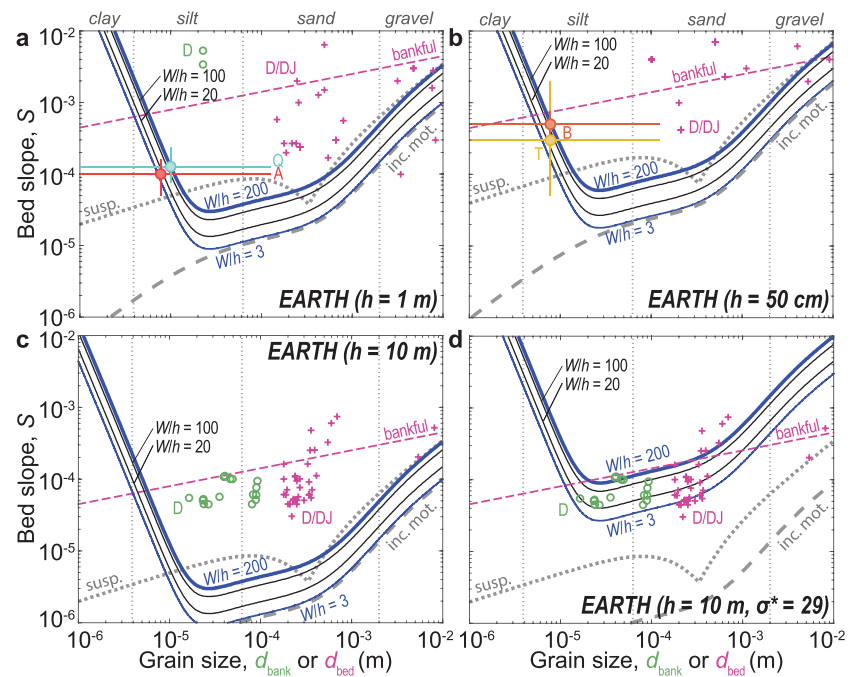


**Figure 4.** Predicted  $W/h$  for terrestrial rivers using input parameters representative of (a) shallow rivers forming within muddy unvegetated banks ( $h = 1$  m;  $Q$  = Quinn River, NV, Matsubara et al., 2015;  $A$  = Amargosa River, CA, Ielpi, 2018a), (b) yet shallower rivers forming within largely plant-devoid banks ( $B$  = washes of the Bonneville Basin, UT, Figure 1a, Ielpi & Lapôtre, 2019a;  $T$  = streams of the Toiyabe Basin, NV, Ielpi & Lapôtre, 2019b), (c) deep rivers ( $h = 10$  m) without modeled vegetation-added bank strength, and (d) deep rivers ( $h = 10$  m) with modeled vegetation-added bank strength ( $\sigma^* = 29$ ). Table 1 summarizes model input parameters for each panel and Table 2 data from natural rivers. In all panels, the approximate stability field for single-thread rivers is indicated by contours of  $W/h$  between 3 and 200. The thresholds of motion (gray dashed lines; Soulsby & Whitehouse, 1997) and of suspension (gray dotted lines; Niño et al., 2003) are added for comparison. In all panels, bank and bed data from vegetated rivers is added for comparison (green circles = bank grain size; pink crosses = bed grain size;  $D$  = Dong et al., 2019;  $DJ$  = Dunne & Jerolmack, 2018). Compiled data with bankfull depths within 10% of the modeled depth ( $h = 0.9$ – $1.1$  m in a;  $h = 0.45$ – $0.55$  m in b;  $h = 9$ – $11$  m in c–d) are included. The pink dashed lines show predictions from the empirical relationship between bankfull Shields stress and bed-specific particle Reynolds number of Trampush et al. (2014) and is to be compared with the bed grain sizes (pink crosses).

model can predict the single-thread-to-braiding transition, it does not apply in the braided regime. Finally, we find that, for siliciclastic grains in freshwater, cohesionless bank materials approach their threshold for incipient motion as  $W/h$  approaches a value of 3 (e.g., Figures 3 and 4). Because bank materials need to be transported in the first place to be deposited overbank, we adopt  $W/h = 3$  as a conservative lower limit for the formation of single-thread rivers.

### 3. Model Results

#### 3.1. General Predictions

For cohesionless sediments, the model of Ternat et al. (2008) shows that the fluid stress required to mobilize grains ( $\tau_0 = \tau_0^*(\rho_s - \rho)gd_{\text{bank}}$ ) generally decreases as  $d_{\text{bank}}$  decreases and follows two different asymptotic behaviors in the hydraulically smooth ( $Re_{p,\text{bank}} < \sim 10^0$ ) and rough ( $Re_{p,\text{bank}} > \sim 10^2$ ) regimes (Figures 2a and 2b). In contrast, the critical stress for erosion of cohesive sediments ( $\tau_{\text{crit}}$ ) increases as  $d_{\text{bank}}$  decreases when cohesion becomes significant (i.e., for mud-sized particles and thus in the smooth regime), such that the critical stress for erosion may be described through three asymptotic regimes as grain size increases—the cohesive-smooth ( $Re_{p,\text{bank}} < Re_{p,c}$ , where typically  $Re_{p,c} < \sim 10^0$ ), transitional ( $Re_{p,c} < Re_{p,\text{bank}} < \sim 10^2$ ), and cohesionless-rough ( $Re_{p,\text{bank}} > \sim 10^2$ ) regimes (Figures 2a and 2b). Because van der Waals forces are a function of the distance between grains, the grain size at which

**Table 1**  
Summary of Parameters Used to Compute Predicted  $W/h$  for Flume Experiments (Figure 3), Terrestrial Rivers (Figure 4), and Martian Rivers (Figures 6 and S2)

Figure	2	3a	3b	3c	3d	4a	4b	4c	4d	6a	S2a	S2b
Flow depth ( $h$ ; m)	1	$6 \times 10^{-3}$	$1.3 \times 10^{-2}$	$7.5 \times 10^{-3}$	$2 \times 10^{-3}$	1	0.5	10	10	1	1	1
Acceleration of gravity ( $g$ ; $m/s^2$ )	9.81	9.81	9.81	9.81	9.81	9.81	9.81	9.81	9.81	3.71	3.71	3.71
Sediment density ( $\rho_s$ ; $kg/m^3$ )	2,650	2,650	1,400 <sup>a</sup>	2,650	1,270 <sup>b</sup>	2,650	2,650	2,650	2,650	2,900	2,900	2,900
Water density ( $\rho$ ; $kg/m^3$ )	1,000	1,000	1,000	1,000	1,000	1,000	1,000	1,000	1,000	1,000	1,000	1,300
Dynamic viscosity ( $\mu$ ; Pa.s)	$1 \times 10^{-3}$	$1 \times 10^{-3}$	$1 \times 10^{-3}$	$1 \times 10^{-3}$	$1 \times 10^{-3}$	$1 \times 10^{-3}$	$1 \times 10^{-3}$	$1 \times 10^{-3}$	$1 \times 10^{-3}$	$1 \times 10^{-3}$	$1.65 \times 10^{-3}$	$5.2 \times 10^{-2}$
Porosity ( $n$ )	0.3	0.5 <sup>c</sup>	0.5 <sup>c</sup>	0.5 <sup>c</sup>	0.5 <sup>c</sup>	0.263 <sup>d</sup>	0.263 <sup>d</sup>					
Strength factor ( $\sigma^*$ )	0	0	0 vs. 1	0	0	0	0	0	29	0	0	0

<sup>a</sup>Published experiments (Braudrick et al., 2009) used both silicate sand and plastic beads. To roughly match the experimental conditions, banks are herein assumed to be made of about 50%-50% of each material, in rough keeping with their Figure 4. <sup>b</sup>Published experiments (Limaye et al., 2018) used two types of plastic beads for their subaerial experiments. To roughly match the experimental conditions, banks are herein assumed to be made of about 50%-50% of each material. <sup>c</sup>Because floodplains were likely not compacted in these experiments, a higher porosity value for the banks is used than for natural rivers, such that cohesion forces only become significant for clay-sized particles in model predictions. <sup>d</sup>This value is chosen to simulate the porosity of a fully compacted arrangement of particles in hexagonal compact packing ( $n_{max} = 0.26$  for perfect spheres).

cohesion becomes negligible (defined by  $d_c = \left(\frac{\nu^2 Re_{pc}^2}{Rg}\right)^{1/3}$ ) is a function of sediment compaction (e.g., Figures 2 vs. 3 vs. 4 and Table 1).

Under steady uniform flow and at constant  $h$ ,  $\tau_{bed}$  (and thus  $\tau_{bank}$ ) is a linear function of bed slope,  $S$ . As such, under our model assumptions, an equilibrium river of fixed  $W/h$  (i.e., for which  $\tau_{bank} = \tau_{crit}$ ) follows three regimes with increasing  $d_{bank}$ —first,  $S$  decreases with increasing  $d_{bank}$  in the cohesive-smooth regime; second,  $S$  increases with coarser bank materials as cohesion becomes negligible in the transitional regime; and third,  $S$  increases more rapidly with  $d_{bank}$  in the cohesionless-rough regime (Figures 2c). In Figure 2c, contours show predicted  $W/h$ , and the  $3 < W/h < 200$  envelope illustrates the stability field of single-thread rivers plotted for typical terrestrial conditions (Table 1; see also Text S4 for a sensitivity analysis). A first important prediction is that single-thread rivers can readily form with fine-grained banks in the absence of bank vegetation. The lower bound for the formation of single-thread rivers corresponds to conditions near the threshold of motion for bank materials when cohesion is negligible because channels with  $W/h \sim 1$  have  $\tau_{bank} \sim \tau_{bed}$  (and by construction  $\tau_{bank} = \tau_{crit}$ ). The majority of the single-thread-river stability field is at bed slopes below the threshold of suspension of the bank materials, except for (i) silt-to-clay-sized particles, which are easily suspended because they are light, and (ii) a narrow grain-size range within the smooth-to-rough transition (with respect to  $Re_{p,bank}$ ; medium sand for siliciclastic grains in ambient freshwater on Earth). Furthermore, the stability field of single-thread rivers is expected to shift to steeper slopes for shallower flows (e.g., Figures 4a vs. 4c), because at constant  $W$ , shallower flows require steeper slopes to achieve  $\tau_{bank} = \tau_{crit}(d_{bank})$ .

### 3.2. Model Tests

### 3.3. Single-Thread and Braided Rivers in Flume Experiments

Here we evaluate the model against results from flume experiments that produced braided and single-thread rivers (Table 2). Peakall et al. (2007) and van Dijk et al. (2012) performed experiments where the sediment supply included mixtures of sand and clay-to-silt-sized silica flour and where banks did not host any vegetation. Both Peakall et al. (2007) and van Dijk et al. (2012) produced single-thread, meandering rivers in their experiments with  $W/h < \sim 20$  and  $\sim 10$ – $30$ , respectively (Figure 3a). Only the experiments of van Dijk et al. (2012), however, were able to produce repeated chute cutoffs. Braudrick et al. (2009) also produced single-thread meandering rivers with  $W/h \sim 30$  by feeding a mixture of 800- $\mu m$  sand and 300- $\mu m$  lightweight plastic particles to the flume and by seeding the floodplain with alfalfa sprouts that added bank strength (Figure 3b).

**Table 2**  
Summary of Data From Flume Experiments and Natural Rivers Used for Comparison With Model Predictions

References [corresponding figure]	van Dijk et al. (2012) [Figure 3a]	Peakall et al. (2007) [Figure 3a]	Braudrick et al. (2009) [Figure 3b]	Moreton et al. (2003) [Figure 3c]	Bertoldi et al. (2009) [Figure 3c]	Limaye et al. (2018) [Figure 3d]	Matsubara and Howard (2014) Matsubara et al. (2015) [Figure 4a]	Ielpi et al. (2018) [Figure 4a]	Ielpi and Lapôtre (2019a) [Figure 4b]	Ielpi and Lapôtre (2019b) [Figure 4b]
Flow depth ( <i>h</i> ; m)	$1.5 \times 10^{-2a}$	$1.5 \times 10^{-2a}$	$1.3 \times 10^{-2}$	$7 \times 10^{-3}$	$< 10^{-2}$	$2 \times 10^{-3}$	1.3	$-1^b$ (0.1–1.2)	$-0.5$ (0.2–1.2)	$-0.5$ (0.2–0.6)
Grain size ( $d_{bank}$ ; $\mu\text{m}$ ) <sup>c</sup>	210 (10–1,000)	380 (10–1,000)	550 (300–800)	780 (~200–1,800)	630	330 (250–420)	$10^d$ (0.98–125)	$8^e$ (0.98–125)	$8^e$ (0.98–125)	$8^e$ (0.98–125)
Bed slope ( <i>S</i> ; %) <sup>f</sup>	0.8 (0.4–1.2)	0.55 (0.28–0.85)	0.52 (0.26–0.78)	1.3 (0.7–2.0)	1.0 (0.7–1.6)	3.5 (1.8–5.0)	0.015 (0.008–0.025)	0.01 (0.005–0.015)	0.05 (0.025–0.075)	0.03 (0.005–0.2)

*Note.* Values in parentheses indicate those used for error bars. <sup>a</sup>Reported values are overall maximum thalweg depths, such that average channel depth in deepest reaches is estimated to half of the reported values, and overall average depth is estimated to be shallower by a few millimeters (consistent with description of Peakall et al., 2007). <sup>b</sup>Reported variability includes many smaller tributary channels. Main trunk channels are overall deeper, with depths consistently  $\sim 1$  m. <sup>c</sup>Reported grain sizes are median sizes (with 10<sup>th</sup> and 90<sup>th</sup> percentiles in parentheses) unless indicated otherwise. <sup>d</sup>A value of 60% silt–40% clay is assumed, as reported for Lake Lahontan sediments. Variable amounts of fine sand were also reported in the banks, although they may be present in lenses and may thus not contribute much to bank cohesion. <sup>e</sup>Although grain-size distributions in the banks were not quantified, they consist of clay and silt with lenses of very fine to fine sand. A value of 50% silt–50% clay is herein assumed as a rough estimate. <sup>f</sup>For slopes, error bars are taken as  $\pm 50\%$  of reported or measured values unless uncertainties/variability are reported in the study.

We also compare model predictions to the experimental braided rivers of Moreton et al. (2002), Bertoldi et al. (2009), and Limaye et al. (2018; Figures 3c–3f and Tables 1 and 2). Specifically, we make predictions of  $W/h$  using  $h$  and  $\rho_s$  values that match those used in the experiments for a range of  $d_{bank}$  and  $S$  and compare our predictions with the  $W/h$  achieved in the experiments at specified values of  $d_{bank}$  and  $S$ .

Model predictions are in agreement with experimental observations within error. The experiments of van Dijk et al. (2012) clearly fall within the predicted stability field of single-thread rivers, and those of Peakall et al. (2007) are close to the braiding-to-single-thread transition (Figure 3a). For Braudrick et al. (2009), we find that the experiment was close to the single-thread river stability regime even without alfalfa sprouts (Figure 3b). Finally, the experiments of Moreton et al. (2002), Bertoldi et al. (2009), and Limaye et al. (2018) produced braided streams with steeper bed slopes and overall higher  $W/h$  ( $\sim 30$ ,  $\sim 50 - 100$ , and  $>100$ , respectively). Consistent with the model, these experiments fall outside of the predicted stability field of single-thread channels (Figures 3c and 3d).

### 3.4. Terrestrial Rivers Forming Within Muddy Unvegetated Banks

Since they evolved over 430 Ma, vascular plants have colonized most terrestrial environments. Thus, there are only few modern examples of single-thread rivers forming with muddy, unvegetated banks on Earth. As a test of the model, we compare predictions against shallow ( $h = 1$  m and  $h = 0.5$  m) rivers that form in mud-prone endorheic basins of the western United States and that are largely devoid of macroscopic plant life (Figures 4a and 4b; Quinn River, NV, Matsubara et al., 2015; Amargosa River, CA, Ielpi, 2018; washes of the Bonneville Basin, UT, Ielpi & Lapôtre, 2019a; streams of the Toiyabe Basin, NV, Ielpi & Lapôtre, 2019b).

Grain sizes in riverbanks of the Amargosa River, Bonneville Basin, and Toiyabe Basin were qualitatively constrained by Ielpi et al. (2018) and Ielpi and Lapôtre (2019a, 2019b) and consist of clay and silt with lenses of very fine to fine sand, similar to Lake Lahontan sediments forming the banks of the Quinn River, NV (Matsubara et al., 2015). The model correctly predicts that the Quinn River, NV, should be single threaded. The model further predicts that both the Amargosa River and washes of the Bonneville Basin should be single threaded, given observed bed slopes, if the effective bank grain size is in the clay-silt range. These effective bank grain sizes are qualitatively consistent with onsite observations and quantitatively consistent with Lake Lahontan sediments incised by the Quinn River in a similar depositional setting.

## 4. Discussion

### 4.1. Quantifying the Effect of Bank Vegetation

Numerical and theoretical models are often used to evaluate the effect of vegetation on bank strength and stream evolution within vegetated banks (e.g., Camporeale et al., 2013; Crosato & Saleh, 2011; Eaton & Giles, 2009; Millar, 2000; Murray & Paola, 2003). Because the theoretical model presented here makes predictions for the formation of single-thread rivers in the absence of vegetation, one can in principle separate the strengthening effects of vegetation on riverbanks from those of sediment properties and quantify them by comparing model predictions with data from vegetated rivers. Specifically,  $\sigma^*$  (equation (10)) can be used to minimize the misfit between predicted and observed  $W/h$ .

To illustrate this application, model predictions are compared with both experimental (Figure 3b) and natural (Figure 4) vegetated single-thread rivers. In the case of the experiments of Braudrick et al. (2009), we find that a moderate increase in the bank-erosion threshold ( $\sigma^* = 1$ ), consistent with the moderate effect of short and shallow-rooted plants on bank strength (e.g., Micheli et al., 2004; Polvi et al., 2014), makes predicted  $W/h$

(shaded green field in Figure 3b) match experimental data. We conduct a similar exercise for natural vegetated single-thread rivers using the compilation of Dong et al. (2019), which includes data from single-threaded reaches of the Selenga River delta (Russia), a set of gravel-bedded rivers from England, the Llano River (United States), the Fly River (Papua New Guinea), and the Siret River (Hungary). Channel reaches from Dong et al. (2019) have  $W/h \sim 4\text{--}136$ ,  $S \sim 2 \times 10^{-5} - 2 \times 10^{-2}$ , and  $d_{\text{bank}} \sim 5\text{--}465 \mu\text{m}$ . The compiled data from vegetated rivers plot within the braided-stability zone of the  $(d_{\text{bank}}, S)$  space (Figure 4) and are predicted to have  $W/h > 200$  in the absence of vegetation, indicating that vegetation is likely an important bank-strengthening agent for these rivers. For example, the banks of the deeper rivers ( $h = 9\text{--}11 \text{ m}$ ; Figure 4c) would need to be composed of clay to fine silt to match model predictions in the absence of vegetation; yet their banks consist of coarse silt to fine sand. An added strength of  $\sigma^* = 29$  due to vegetation allows model predictions to match observations (Figure 4d), consistent with the strengthening effect of riparian shrubs and trees (Polvi et al., 2014; Smith, 1976).

#### 4.2. Hydraulic Geometry of Single-Thread Rivers Forming Within Muddy Unvegetated Banks

Terrestrial rivers were shown to adjust their bankfull geometry such that their formative Shields stress ( $\tau^* = \frac{\tau_{\text{bed}}}{(\rho_s - \rho)gd_{\text{bed}}}$ ) decreases with the particle Reynolds number ( $\text{Re}_{\text{p,bed}} = \frac{(Rgd_{\text{bed}}^3)^{1/2}}{\nu}$ ) approximately as

$$\tau^* \propto \text{Re}_{\text{p,bed}}^{-1/2} \quad (11)$$

(pink dashed line in Figure 4; Parker et al., 2007; Wilkerson & Parker, 2010; Trampus et al., 2014). This empirical relationship predicts relatively accurately the bankfull geometry of vegetated rivers (Figure 4). Similar empirical relationships are often used to infer paleohydraulic conditions from fluvial deposits on Earth (e.g., Mahon & McElroy, 2018) and Mars (e.g., Jacobsen & Burr, 2016). However, the degree to which such relationships may be applied to unvegetated systems, such as pre-Silurian (e.g., Eriksson et al., 2006; Mukhopadhyay et al., 2014) or Martian (e.g., Jacobsen & Burr, 2018) rivers, is not well understood. Moreover, bank cohesion is not accounted for under this choice of dimensionless variables, and significant scatter remains around the derived relationship (e.g., Wilkerson & Parker, 2010).

Single-thread rivers forming within muddy unvegetated banks (Figures 4a and 4b) are good systems to test the importance of bank cohesion on bankfull geometry. The compiled rivers (Amargosa River, Quinn River, washes of the Bonneville Basin, and streams of the Toiyabe Basin) have fine grains on their beds (silt to medium sand), such that their formative Shields stresses fall within the scatter of vegetated rivers (pink crosses in Figures 4a and 4b). Therefore, unvegetated and vegetated rivers on Earth seem to have statistically similar hydraulic geometries (Ielpi et al., 2017), and terrestrial unvegetated single-thread rivers might be described well by equation (11). For rivers with cohesive banks, bankfull geometry is perhaps more intuitively described using a bank-specific Shields stress ( $\tau_{*,\text{bank}} \sim \frac{hS}{Rd_{\text{bank}}}$ ) and a bank-specific particle Reynolds number ( $\text{Re}_{\text{p,bank}} = \frac{(Rgd_{\text{bank}}^3)^{1/2}}{\nu}$ ; e.g., Li et al., 2015). However, in the cohesive limit, the formative  $\tau_{*,\text{bank}}$  is not solely a function of  $\text{Re}_{\text{p,bank}}$ , and another dimensionless number ( $\Omega$ ) is required to describe cohesion (equation (9)). In the cohesive limit,  $\tau_{*,\text{bank}} \propto \Omega \text{Re}_{\text{p,bank}}^{-2}$ , such that the equilibrium bed slope for a given  $W$  and  $h$  is expected to be proportional to  $d_{\text{bank}}^{-3}$  in the cohesive regime (e.g., Figure 4); conversely, at constant  $S$ ,  $W/h$  is expected to increase with increasing  $d_{\text{bank}}$ . The latter prediction is qualitatively consistent with the analysis of the vegetated Selenga River delta of Dong et al. (2019). In summary, the equilibrium bankfull geometry of single-thread rivers forming in unvegetated cohesive sediments is expected to be a strong function of bank grain size.

Single-thread rivers forming within muddy unvegetated banks (Figures 4a and 4b) are good systems to test the importance of bank cohesion on bankfull geometry. The compiled rivers (Amargosa River, Quinn River, washes of the Bonneville Basin, and streams of the Toiyabe Basin) have fine grains on their beds (silt to medium sand), such that their formative Shields stresses fall within the scatter of vegetated rivers (pink crosses in Figures 4a and 4b). Therefore, unvegetated and vegetated rivers on Earth seem to have statistically similar hydraulic geometries (Ielpi et al., 2017), and terrestrial unvegetated single-thread rivers might be described well by equation (11). For rivers with cohesive banks, bankfull geometry is perhaps more intuitively described using a bank-specific Shields stress ( $\tau_{*,\text{bank}} \sim \frac{hS}{Rd_{\text{bank}}}$ ) and a bank-specific particle Reynolds number ( $\text{Re}_{\text{p,bank}} = \frac{(Rgd_{\text{bank}}^3)^{1/2}}{\nu}$ ; e.g., Li et al., 2015). However, in the cohesive limit, the formative  $\tau_{*,\text{bank}}$  is not solely a function of  $\text{Re}_{\text{p,bank}}$ , and another dimensionless number ( $\Omega$ ) is required to describe cohesion (equation (9)). In the cohesive limit,  $\tau_{*,\text{bank}} \propto \Omega \text{Re}_{\text{p,bank}}^{-2}$ , such that the equilibrium bed slope for a given  $W$  and  $h$  is expected to be proportional to  $d_{\text{bank}}^{-3}$  in the cohesive regime (e.g., Figure 4); conversely, at constant  $S$ ,  $W/h$  is expected to increase with increasing  $d_{\text{bank}}$ . The latter prediction is qualitatively consistent with the analysis of the vegetated Selenga River delta of Dong et al. (2019). In summary, the equilibrium bankfull geometry of single-thread rivers forming in unvegetated cohesive sediments is expected to be a strong function of bank grain size.

#### 4.3. Applications to Pre-Silurian River Deposits

Few single-thread river systems have been reported relative to braided systems in the pre-Silurian sedimentary record based on the presence of heterolithic lateral accretion sets (e.g., Gibling et al., 2014). Whereas global compilations show that the rise of land plants brought about a sharp increase in mud content within preserved fluvial deposits (McMahon & Davies, 2018a), endorheic basins capable of

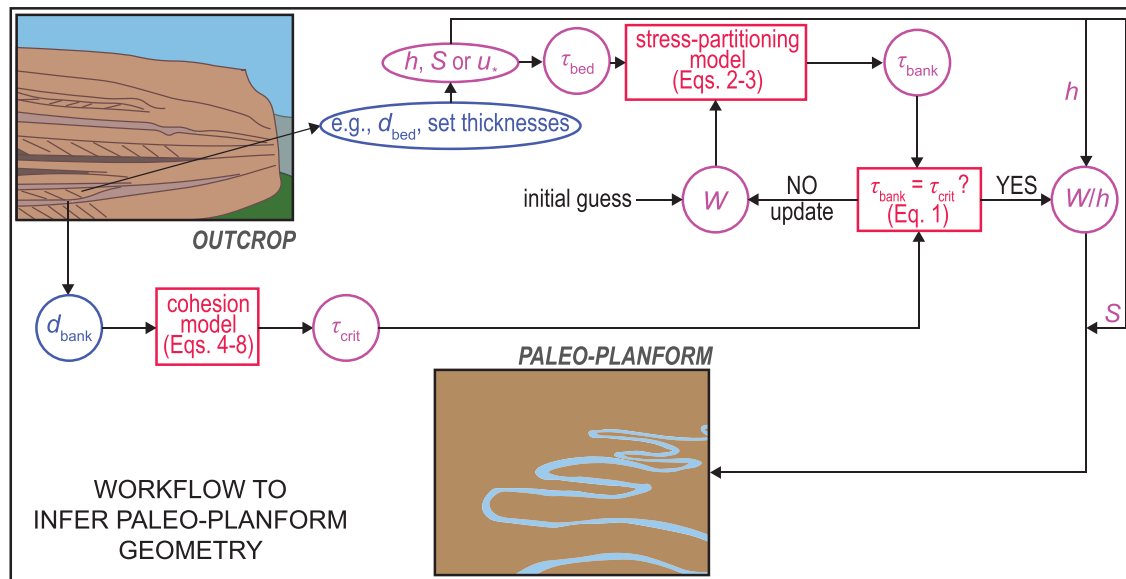


**Figure 5.** Conceptual workflow to infer paleo-planform geometry of rivers from outcrop observations of ancient fluvial deposits.

retaining mud fractions from oceanward transport (e.g., Dott, 2003) should also have formed before the rise of land plants and provided favorable geodynamic and paleoclimatic settings for the accumulation of mud (Nichols, 2012). In a compilation of prevegetation fluvial floodplain deposits, Ielpi et al. (2018) envisaged a causal link between the rise of supercontinental assemblages, the thorough chemical weathering of large orogenic belts therein, and the deposition of mud-rich strata in low-gradient, endorheic-prone terrestrial basins. Moreover, analyses of fine-grained Proterozoic sedimentary rocks show that both detrital and pedogenic clays were produced abundantly more than a billion years before the rise of land plants (Tosca et al., 2010). Thus, despite a reported paucity of mudrocks in the identified pre-Silurian fluvial record, there is no a priori reason why single-thread rivers should have been rare on the pre-Silurian Earth. In fact, several single-thread river deposits have been identified in strata that predate the greening of the continents based on detailed observations of point bars and channel fills (Long, 1978, 2011; Ielpi & Rainbird, 2015; Santos & Owen, 2016; Ielpi et al., 2016, 2017) as well as dune cross stratification (e.g., Ganti et al., 2019).

Combining our model predictions with a dune-stability criterion (Lapôtre et al., 2017), we show that riverbanks need strength for dunes to form in coarse-sand or finer beds (Text S5 and Figure S1), consistent with the recent analysis of Ganti et al. (2019) of prevegetation fluvial deposits of the Torridon Group of Scotland. The question remains, however, of what strengthened pre-Silurian riverbanks. Mud contents as low as 3% by weight cause sand/mud mixtures to become cohesive, with cohesion increasing nearly linearly with mud content up to ~20–30% mud (Mitchener & Torfs, 1996; Ternat et al., 2008). It is thus possible that some of the observed sandy deposits are in fact floodplain deposits, and small amounts of mud were either removed or overlooked. This idea is consistent with recent observations of a modern point-bar deposit along a highly mobile unvegetated river meander in the Toiyabe Basin, NV (Ielpi & Lapôtre, 2019b), which is dominated by sand-sized materials with little intercalated mud. If found to be representative of other unvegetated meandering streams, the observed stratigraphy in the Toiyabe Basin is inconsistent with heterolithic lateral accretion sets being diagnostic of river meandering (as also suggested by, e.g., Hartley et al., 2018; McMahon & Davies, 2018b; Swan et al., 2018).

In the absence of clear heterolithic lateral accretion sets, the deposits of pre-Silurian rivers may preserve indirect clues about bank materials and channel width that our model can help decipher (Figure 5). First, one may use our model to infer the effective grain size of bank materials based on observations of channel deposits. In the case of polydisperse riverbanks, the effective grain size inferred through our model would

reflect the sediment size that would yield the same bank strength as the true banks. Thus, an inverted grain size in the clay-to-silt range would suggest that banks were eroding cohesively and thus that some amount of mud (>3%; Mitchener & Torfs, 1996; Ternat et al., 2008) was likely present. For example, Ganti et al. (2019) independently determined that rivers that formed the Upper Applecross Formation of the Torridon Group in Scotland had typical depths of ~10 m and bed slopes of  $\sim 10^{-4}$ . They also inferred that those streams were single threaded. Our model suggests that such deposits can be explained by flows confined within banks composed of sediments with an effective grain size of  $\sim 3\text{--}8\ \mu\text{m}$  or in the clay-to-silt range and thus that mud could have strengthened the riverbanks (Figure 4c). Although fine-grained floodplain deposits are not abundant, pre-Silurian alluvial strata typically contain a few percent mudrock (McMahon & Davies, 2018a), and the grain size of fines in putative bank-forming materials can be estimated from fine-grained intervals or lenses in the otherwise sand-dominated deposits. Using the full formulation of Ternat et al. (2008) for polydisperse sediments and observations of fine-grained intervals in the Torridon deposits, one could quantitatively determine the amount of mud required to produce the bank strength equivalent to 3- to 8- $\mu\text{m}$  grains.

Second, it is difficult to determine channel width in the absence of floodplain sediments in pre-Silurian fluvial strata. Flow depth and bed stress can be characterized by inspection of bedforms and barforms within channel deposits and used in a stress-partitioning model to estimate bank stresses (equations (2) and (3)). Bank-strengthening grain sizes can be estimated by inspection of fine intervals and fed into a bank-cohesion model (equations (4)–(8)). Paleo-channel width can then be estimated by iteratively solving equation (1), using the inferred  $W/h$  combined with estimates of paleo-bed slope (e.g., from bed stress estimates, bed grain size, and flow depth; Lynds et al., 2014; Trampush et al., 2014; Mahon & McElroy, 2018; Figure 5). For example, consider a putative ancient channel-bed deposit from an Amargosa-like river (Ielpi, 2018), with grain sizes of  $\sim 100\ \mu\text{m}$  and that contains  $\sim 1\text{-m}$ -tall bar forms and current ripples with wavelengths of  $\sim 11\ \text{cm}$ . Using the formulation of Lapôtre et al. (2017), we determine that the formation of 11-cm ripples in 100- $\mu\text{m}$  grains required bed stresses of  $\tau_b \sim 0.6\ \text{Pa}$ . Further assuming that bar height can be used as a 1:1 proxy for flow depth,  $h$ , bed slope can be estimated under steady uniform flow conditions as  $S = \frac{\tau_b}{\rho gh} \approx 6 \times 10^{-5}$ . The ancient Amargosa-like deposit also contains homogeneously fine-grained intervals in the form of mud drapes. Assuming that they are representative of sediments that provided strength to the riverbanks, bank grain size can be estimated by inspection of those fine intervals. For a bank grain size of  $\sim 10\ \mu\text{m}$ , our model would predict that the river that formed the observed deposits had a  $W/h \approx 20$  or a channel width of  $\sim 20\ \text{m}$  (Figure 4a). If instead the finest intervals had a grain size of  $\sim 50\ \mu\text{m}$ , our model would predict an equilibrium  $W/h > 200$ , indicating the rocks were deposited by a braided river (Figure 4a).

#### 4.4. Single-Thread Rivers on Early Mars and Implications for Climate Scenarios

In order to illustrate how the ancient Martian environment may have influenced the formation of single-thread rivers, predicted  $W/h$  are shown for a shallow Martian river ( $h = 1\ \text{m}$ ), where only gravity and the density of sediments (quartz-dominated on Earth vs. basaltic on Mars) were varied relative to their terrestrial equivalents (Figure 6a and Table 1; see also Text S6 and Figure S2). Although Martian clays are dominated by Fe/Mg rich minerals (e.g., Ehlmann & Edwards, 2014; Mustard et al., 2008; Poulet et al., 2005), the effect of clay mineralogy is ignored here (Text S2). Compared to terrestrial rivers, Martian single-thread rivers are predicted to form at steeper bed slopes (Figure 6a). Intuitively, the lower Martian gravity implies lower bed stresses at a given slope, such that achieving similar bank stresses on both planets requires steeper riverbeds on Mars. In addition, the degree to which a Martian river must steepen to achieve Earth-like bank stresses is not the same for all bank materials. By Taylor expansion of  $\tau_{\text{crit}}^*$  ( $\text{Re}_{p,\text{bank}}$ ) (equations (5) and (9)), we find that for a given grain size, Martian rivers (relative to their terrestrial counterparts) are expected to have slopes  $\sim \frac{g_E}{g_M} \approx 2.6$  times steeper in the smooth-cohesive limit (because of the lower Martian gravity) and  $\sim \frac{\rho_M}{\rho_E} \approx 1.2$  times steeper in the cohesionless-rough limit (because of the higher density of basaltic sediments) but to have similar slopes in the transitional regime (where subscripts “E” and “M” indicate Earth and Mars, respectively; Figure 6).

Shifting the stability domain of single-thread rivers to steeper equilibrium slopes is equivalent to forming narrower rivers on Mars at a given bed slope. Figure 6b shows the ratio of predicted Martian-to-

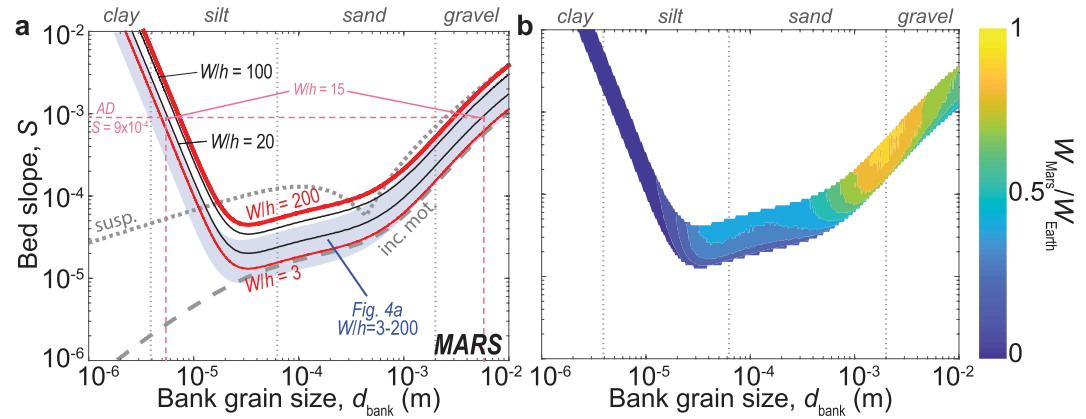


**Figure 6.** (a) Predicted  $W/h$  on Mars assuming the density and dynamic viscosity of freshwater at 25 °C ( $h = 1$  m). Table 1 summarizes model input parameters. The approximate stability field for single-thread rivers is indicated by contours of  $W/h$  between 3 and 200. The thresholds of motion (gray dashed lines; Soulsby & Whitehouse, 1997) and of suspension (gray dotted lines; Niño et al., 2003) are added for comparison. The blue shaded area highlights the corresponding  $W/h = 3-200$  contours under Earth's gravity (Figure 4a). The pink dashed lines illustrate how to invert for bank-sediment grain size from estimates of channel bed slope at Aeolis Dorsa (AD). (b) Predicted ratio of Martian-to-terrestrial river widths as a function of  $d_{\text{bank}}$  and  $S$  for  $h = 1$  m. Ratio is only shown where predicted  $W/h$  is less than 200 on Mars.

terrestrial channel widths ( $\frac{W_M}{W_E}$ ) as a function of  $d_{\text{bank}}$  and  $S$ . Consistent with the previous analysis, at constant  $d_{\text{bank}}$  and  $S$ , Martian rivers are found to be significantly narrower than their terrestrial counterparts ( $\frac{W_M}{W_E} \approx 0.1$ ) in the smooth-cohesive regime, whereas Martian rivers have similar equilibrium widths in the transitional regime and again become moderately narrower than terrestrial rivers in the cohesionless-rough regime ( $\frac{W_M}{W_E} \approx 0.6$  within fine-gravel banks; Figure 6b).

Our model predictions are qualitatively consistent with the inference of Konsoer et al. (2018) that Martian rivers must have steeper beds than terrestrial rivers of similar  $W/h$ . Specifically, Konsoer et al. (2018) proposed empirical relationships to predict bankfull depth ( $h$ ) and flow discharge ( $Q_0$ ) from channel width on Mars,

$$h = 0.164W^{0.66}, \quad (12)$$

and

$$Q_0 = 0.2W^{1.68}. \quad (13)$$

Assuming steady uniform flow and a constant dimensionless bed-friction factor ( $C_f$ ), bankfull discharge for a rectangular channel may be rewritten as

$$Q_0 = W \sqrt{\frac{gh^3 S}{C_f}}, \quad (14)$$

such that bed slope can be found as a function of  $W$  by combining equations (12)–(14) as

$$S \approx 9.1 \frac{C_f}{g} W^{-0.62}. \quad (15)$$

Provided that  $W$  can be estimated from orbiter-based imagery, equations (12) and (15) can be used to determine  $W/h$  and  $S$ , which then can be combined with our model to determine  $d_{\text{bank}}$ . For example, Kite et al. (2015) measured ridge widths between  $\sim 10$  and  $\sim 50$  m at Aeolis Dorsa and assumed these were equivalent to channel widths. Combined with equation (12), the estimates of Kite et al. (2015) imply channel depths of

$\sim 0.75\text{--}2.2$  m or  $W/h \sim 13\text{--}23$ . Further assuming  $C_f \approx 2 \times 10^{-3}$  (Wright & Parker, 2004), equation (15) constrains channel paleo-slopes to be  $\sim 4.3 \times 10^{-4} - 1.2 \times 10^{-3}$  at Aeolis Dorsa, in agreement with the independent estimates of  $5 \times 10^{-4} - 1 \times 10^{-3}$  from DiBiase et al. (2013) for ridges in the same area. Using these values, our model predicts that Aeolis Dorsa rivers must have flowed within banks whose eroding behavior was equivalent to that of either fine silt or fine gravel (illustrated in Figure 6a for representative values of  $h \sim 1$  m and  $W \sim 15$  m and with  $S \sim 9 \times 10^{-4}$ ). Fine-grained banks are more consistent with the now wind-eroded floodplains that led to ridge formation.

Even though floodplain deposits were preferentially eroded to form Martian sinuous ridges, detrital cohesive fine-grained sediments have been observed by the National Aeronautics and Space Administration's (NASA) Curiosity rover within Gale crater (e.g., Bristow et al., 2018; Grotzinger et al., 2015; Schieber et al., 2017). In addition, the global abundance of clay minerals as detected by orbiter-based spectrometers in Late-Noachian-to-Early-Hesperian terrains (Ehlmann & Edwards, 2014; Mustard et al., 2008; Poulet et al., 2005) attests to significant clay production in the early history of Mars. Provided observations of bank-materials grain sizes from Martian river deposits, possibly as early as the 2020s when NASA's next rover will investigate a river delta deposit within Jezero crater (e.g., Goudge et al., 2017; Schon et al., 2012), our model can be used to evaluate whether mud in riverbanks can explain the origin of single-thread rivers and as a paleohydraulic tool to decipher ancient Martian fluvial deposits (Text S6 and Figure S2). Determining the bank materials of ancient Martian rivers is important for the hydrologic and climate history of Early Mars—clays imply silicate weathering which in turn could indicate warmer surface temperatures during channel-forming episodes (e.g., Bishop et al., 2018; Carter et al., 2015) relative to an ice-cemented, mud-free scenario, which instead would imply near-freezing surface conditions with only limited silicate weathering at the surface. Alternatively, chemical cements would likely imply a net evaporative surface environment.

## 5. Conclusions

Single-thread river systems are a conspicuous part of Earth's land surface today. A strong spatiotemporal correlation between the occurrence of single-thread rivers and vegetation supports the hypothesis that land-plant evolution has influenced the development of fluvial systems through time. Despite this correlation, a few single-thread-river deposits have been recognized in the fluvial rock record prior to the advent of land plants, and meandering-river deposits are found in vegetation-free basins on Earth and on Mars, where macroscopic plants most likely never evolved. Thus, although vegetation may have played an important role in shaping Earth's rivers, rivers do not require vegetation to be single threaded. Here we explore whether cohesive mud may provide riverbanks with sufficient resistance to erosion for flows to be confined within relatively deep and narrow channels without vegetation. We combine equations of open-channel flow hydraulics with a physics-based erosion model that is applicable to a broad range of bank sediments. The new model permits us to make predictions of river width-to-depth ratio ( $W/h$ ), which correlates with its planform geometry. The model predicts that single-thread rivers can form with a broad range of bank substrates, from clay to gravel banks, consistent with rivers formed in flume experiments and within largely unvegetated mud-prone endorheic basins of the western United States.

The model has several useful applications. First, we show how the model can be used to infer the strengthening effect of vegetation on riverbanks by quantifying the contribution of mud cohesion. Second, we discuss possible controls on bankfull hydraulic geometry of single-thread rivers with muddy unvegetated banks and show that width should be a strong function of bank grain size. Third, in application to pre-Silurian fluvial deposits, we propose a workflow to determine bank strength (and thus the effective grain size of bank materials) or reconstruct a river's planform geometry from a simple set of field observables (grain size, bedforms, etc.). This workflow holds promise in deciphering indirect clues from the pre-Silurian fluvial record. Finally, we show that single-thread rivers are predicted to form within a broad range of bank materials on Mars. Owing to lower gravity, Martian rivers are expected to be narrower than their terrestrial counterparts at a given slope. Conversely, rivers of a given width are expected to have steeper bed slopes on Mars in order to achieve the necessary bank stresses to cause bank erosion. Future in situ observations of Martian

single-thread-river deposits can be used with our model to constrain whether sufficient bank strength was provided by mud. If not, chemical cements or ground ice may have played an important role in forming meandering rivers on Early Mars.

### Data Availability Statement

All data underlying the paper were published prior to our study (Moreton et al., 2003; Peakall et al., 2007; Bertoldi et al., 2009; Braudrick et al., 2009; van Dijk et al., 2012; DiBiase et al., 2013; Matsubara & Howard, 2014; Kite et al., 2015; Matsubara et al., 2015; Ielpi, 2018; Limaye et al., 2018; Ielpi & Lapôtre, 2019a, 2019b), are cited throughout where appropriate, and can be accessed directly through cited references.

**Table A1**  
*List of Notations Used in the Present Study*

Symbol	Variable
$A_H$	Hamaker constant
$c$	Cohesion (Pa)
$C_f$	Dimensionless bed-friction coefficient
$d_{\text{bank}}$	Bank grain size (m)
$d_{\text{bed}}$	Bed grain size (m)
$d_c$	Bank grain size defining the cohesive-cohesionless transition (m)
$F_c$	Intergranular cohesion force (N)
$F_d$	Drag force exerted by fluid flow on a grain (N)
$F_l$	Lift force exerted by fluid flow on a grain
$F_w$	Weight of a grain (N)
$Fr$	Froude number
$g$	Acceleration of gravity ( $\text{m/s}^2$ )
$g_E$	Terrestrial acceleration of gravity ( $\text{m/s}^2$ )
$g_M$	Martian acceleration of gravity ( $\text{m/s}^2$ )
$h$	Bankfull channel depth (m)
$K_n$	Compaction function (equation (8))
$k_w$	Grain shape factor
$n$	Sediment porosity (%)
$n_c$	Fully compacted sediment porosity (%)
$n_{\text{max}}$	Maximum sediment porosity (%)
$Q_0$	Bankfull flow discharge ( $\text{m}^3/\text{s}$ )
$R$	Specific submerged density of the sediment
$R_E$	Terrestrial specific submerged density of the sediment
$R_M$	Martian specific submerged density of the sediment
$Re_{p,\text{bank}}$	Bank-specific particle Reynolds number
$Re_{p,\text{bed}}$	Bed-specific particle Reynolds number
$Re_{p,c}$	Bank-specific particle Reynolds number defining the cohesive-cohesionless transition
$S$	Bed slope
$u^*$	Fluid shear velocity (m/s)
$W$	Bankfull channel width (m)
$W/h$	River width-to-depth ratio
$W_E$	Terrestrial channel width (m)
$W_M$	Martian channel width (m)
$W^*$	Threshold width-to-depth ratio for meandering
$\beta$	Grain coordination number
$\epsilon$	Stress-partitioning function
$\mu$	Dynamic viscosity (Pa.s)
$\nu$	Kinematic viscosity ( $\text{m}^2/\text{s}$ )
$\rho$	Fluid density ( $\text{kg/m}^3$ )
$\rho_s$	Sediment density ( $\text{kg/m}^3$ )
$\sigma^*$	Dimensionless strength factor
$\sigma_n$	Normal stress (Pa)
$\tau$	Shear stress (Pa)
$\tau_{\text{bank}}$	Shear stress exerted by the flow on riverbanks (Pa)
$\tau_{\text{bed}}$	Shear stress exerted by the flow on the bed (Pa)

**Table A1** (continued)

Symbol	Variable
$\tau_{\text{crit}}$	Critical shear stress for the erosion of bank materials (Pa)
$\tau_{\text{veg}}$	Vegetation-added stress required to erode bank materials (Pa)
$\tau^*$	Shields stress
$\tau^*_{\text{bank}}$	Bank-specific Shields stress
$\tau^*_0$	Critical Shields stress for the incipient motion of loose grains
$\tau^*_{\text{crit}}$	Dimensionless critical shear stress for the erosion of bank materials
$\tau^*_{\text{crit,total}}$	Dimensionless critical shear stress for the erosion of vegetated bank materials
$\tau^*_{\text{veg}}$	Dimensionless vegetation-added stress required to erode bank materials
$\phi$	Angle of friction (not in the Mohr-Coulomb sense, see text)
$\Omega$	Dimensionless number describing the relative energies of van der Waals forces and grain-scale turbulent eddies

## Appendix A

### Acknowledgments

We thank four anonymous reviewers, B. McElroy, and the Associate Editor for thorough and insightful reviews, and A. J. F. Hoitink for editorial handling of our manuscript. M. Lapôtre was supported by the John Harvard Distinguished Science Fellowship Program within the FAS Division of Science of Harvard University. A. Ielpi was supported by a Discovery Grant from the Natural Sciences and Engineering Research Council of Canada. A. Knoll thanks the NASA Astrobiology Institute.

### References

- Abdullatif, O. M. (1989). Channel-fill and sheet-flood facies sequences in the ephemeral terminal River Gash, Kassala, Sudan. *Sedimentary Geology*, *63*, 171–184.
- Ashmore, P. (1991). Channel morphology and bedload pulses in braided, gravel-bed streams. *Geografiska Annaler*, *73A*, 37–52.
- Bathurst, J. C., Thorne, C. R., & Hey, R. D. (1977). Direct measurements of secondary currents in river bends. *Nature*, *269*, 504–506.
- Bertoldi, W., Zanoni, L., & Tubino, M. (2009). Planform dynamics of braided streams. *Earth Surface Processes & Landforms*, *34*, 547–557. <https://doi.org/10.1002/esp.1755>
- Bishop, J. L., Fairen, A. G., Michalski, J. R., Gago-Duport, L., Baker, L. L., Velbel, M. A., et al. (2018). Surface clay formation during short-term warmer and wetter conditions on a largely cold ancient Mars. *Nature Astronomy*, *2*, 206–213. <https://doi.org/10.1038/s41550-017-0377-9>
- Bluck, B. J. (1971). Sedimentation in the meandering River Endrick. *Scottish Journal of Geology*, *7*, 93–138.
- Bluck, B. J. (1974). Structure and directional properties of some valley sandur deposits in southern Iceland. *Sedimentology*, *21*, 533–554.
- Bradley, R. W., & Venditti, J. G. (2019). Transport scaling of dune dimensions in shallow flows. *Journal of Geophysical Research: Earth Surface*, *124*(2), 526–547. <https://doi.org/10.1029/2018JF004835>
- Braudrick, C. A., Dietrich, W. E., Leverich, G. T., & Sklar, L. S. (2009). Experimental evidence for the conditions necessary to sustain meandering in coarse-bedded rivers. *Proceedings of the National Academy of Sciences*, *106*, 16,936–16,941. <https://doi.org/10.1073/pnas.0909417106>
- Bristow, T. F., Rampe, E. B., Achilles, C. N., Blake, D. F., Chipera, S. J., Craig, P., et al. (2018). Clay mineral diversity and abundance in sedimentary rocks of Gale crater, Mars. *Science Advances*, *4*(6). <https://doi.org/10.1126/sciadv.aar3330>
- Bui, T. D., Laursen, E. M., & Millar, R. G. (2000). Stable width and depth of gravel-bed rivers with cohesive banks. *Journal of Hydraulic Engineering*, *126*, 164–166.
- Burr, D. M., Williams, R. M., Wendell, K. D., Chojnacki, M., & Emery, J. P. (2010). Inverted fluvial features in the Aeolis/Zephyria Plana region, Mars: Formation mechanism and initial paleodischarge estimates. *Journal of Geophysical Research*, *115*(E7). <https://doi.org/10.1029/2009JE003496>
- Camporeale, C., Perucca, E., Ridolfi, L., & Gurnell, A. M. (2013). Modeling the interactions between river morphodynamics and riparian vegetation. *Reviews of Geophysics*, *51*, 379–414. <https://doi.org/10.1002/rog.20014>
- Cardenas, B. T., Mohrig, D., & Goudge, T. A. (2018). Fluvial stratigraphy of valley fills at Aeolis Dorsa, Mars: Evidence for base-level fluctuations controlled by a downstream water body. *Bulletin of the Geological Society of America*, *130*(3-4), 484–498. <https://doi.org/10.1130/B31567.1>
- Carter, J., Loizeau, D., Mangold, N., Poulet, F., & Bibring, J.-P. (2015). Widespread surface weathering on early Mars: A case for a warmer and wetter climate. *Icarus*, *248*, 373–382. <https://doi.org/10.1016/j.icarus.2014.11.011>
- Cotter, E. (1978). The evolution of fluvial style, with special reference to the central Appalachian Paleozoic. In A. D. Miall (Ed.), *Fluvial sedimentology* (Vol. 5, pp. 361–383). Calgary, Canada: Canadian Society of Petroleum Geologists.
- Crosato, A., & Mosselman, E. (2009). Simple physics-based predictor for the number of river bars and the transition between meandering and braiding. *Water Resources Research*, *45*, W03424. <https://doi.org/10.1029/2008WR007242>
- Crosato, A., & Saleh, M. S. (2011). Numerical study on the effects of floodplain vegetation on river planform style. *Earth Surface Processes & Landforms*, *36*, 711–720. <https://doi.org/10.1002/esp.2088>
- Davies, N. S., & Gibling, M. R. (2010). Cambrian to Devonian evolution of alluvial systems: The sedimentological impact of the earliest land plants. *Earth-Science Reviews*, *98*(3-4), 171–200. <https://doi.org/10.1016/j.earscirev.2009.11.002>
- Davies, N. S., Gibling, M. R., & Rygel, M. C. (2011). Alluvial facies evolution during the Palaeozoic greening of the continents: Case studies, conceptual models and modern analogues. *Sedimentology*, *58*(1), 220–258. <https://doi.org/10.1111/j.1365-3091.2010.01215.x>
- de Almeida, R. P., Marconato, A., Freitas, B. T., & Turra, B. B. (2016). The ancestors of meandering rivers. *Geology*, *44*, 203–206. <https://doi.org/10.1130/G37534.1>

- Di Achille, G., & Hynek, B. M. (2010). Ancient ocean on Mars supported by global distribution of deltas and valleys. *Nature Geoscience*, 3, 459–463. <https://doi.org/10.1038/NGEO891>
- DiBiase, R. A., Limaye, A. B., Scheingross, J. S., Fischer, W. W., & Lamb, M. P. (2013). Deltaic deposits at Aeolis Dorsa: Sedimentary evidence for a standing body of water on the northern plains of Mars. *Journal of Geophysical Research: Planets*, 118, 1285–1302. <https://doi.org/10.1002/jgre.20100>
- Dietrich, W. E., & Perron, J. T. (2006). The search for a topographic signature of life. *Nature*, 439, 411–418. <https://doi.org/10.1038/nature04452>
- Dietrich, W. E., Smith, J. D., & Dunne, T. (1979). Flow and sediment transport in a sand bedded meander. *Journal of Geology*, 87, 305–315.
- Dong, T. Y., Nittrouer, J. A., Czapiga, M. J., Ma, H., McElroy, B., Il'icheva, E., et al. (2019). Roles of bank materials in setting bankfull hydraulic geometry as informed by the Selenga River delta, Russia. *Water Resources Research*, 55(1), 827–846. <https://doi.org/10.1029/2017WR021985>
- Dott, R. H. Jr. (2003). The importance of eolian abrasion in supermature quartz sandstones and the paradox of weathering on vegetation-free landscapes. *Journal of Geology*, 111(4), 387–405. <https://doi.org/10.1086/375286>
- Dunne, K. B., & Jerolmack, D. J. (2018). Evidence of, and a proposed explanation for, bimodal transport states in alluvial rivers. *Earth Surface Dynamics*, 6, 583–594. <https://doi.org/10.5194/esurf-6-583-2018>
- Eaton, B. C., Church, M., & Davies, T. R. H. (2006). A conceptual model for meander initiation in bedload-dominated streams. *Earth Surface Processes & Landforms*, 31, 875–891. <https://doi.org/10.1002/esp.1297>
- Eaton, B. C., Church, M., & Millar, R. G. (2004). Rational regime model of alluvial channel morphology and response. *Earth Surface Processes & Landforms*, 26(4), 511–529. <https://doi.org/10.1002/esp.1062>
- Eaton, B. C., & Giles, T. R. (2009). Assessing the effect of vegetation-related bank strength on channel morphology and stability in gravel-bed streams using numerical models. *Earth Surface Processes & Landforms*, 34(5), 712–724. <https://doi.org/10.1002/esp.1768>
- Ehlmann, B. L., & Edwards, C. S. (2014). Mineralogy of the Martian surface. *Annual Reviews of Earth & Planetary Sciences*, 42, 291–315. <https://doi.org/10.1146/annurev-earth-060313-055024>
- Ehlmann, B. L., Mustard, J. F., Murchie, S. L., Poulet, F., Bishop, J., Brown, A. J., et al. (2008). Orbital identification of carbonate-bearing rocks on Mars. *Science*, 322, 1828–1832. <https://doi.org/10.1126/science.1164759>
- Engelund, F., & Skovgaard, O. (1973). On the origin of meandering and braiding in alluvial streams. *Journal of Fluid Mechanics*, 57, 289–302.
- Eriksson, P. G., Bumby, A. J., Brümer, J. J., & van der Neut, M. (2006). Precambrian fluvial deposits: Enigmatic palaeohydrological data from the c. 2–1.9 Ga Waterberg Group, South Africa. *Sedimentary Geology*, 190(1–4), 25–46. <https://doi.org/10.1016/j.sedgeo.2006.05.003>
- Fassett, C. I., & Head, J. W. III (2008). Valley network-fed, open-basin lakes on Mars: Distribution and implications for Noachian surface and subsurface hydrology. *Icarus*, 198, 37–56. <https://doi.org/10.1016/j.icarus.2008.06.016>
- Ferguson, R. (1987). Hydraulic and sedimentary controls of channel pattern. In K. Richards (Ed.), *River channels: Environment and process* (pp. 129–158). Oxford, UK: Blackwell.
- Flintham, T., & Carling, P. (1988). Prediction of mean bed and wall boundary shear in uniform and compositely rough channels. In W. P. White (Ed.), *Proceedings international conference on river regime* (pp. 267–287). Chichester, UK: John Wiley.
- Ganti, V., Whittaker, A. C., Lamb, M. P., & Fischer, W. W. (2019). Low gradient, single-threaded rivers prior to greening of the continents. *Proceedings of the National Academy of Science*, 116(24). <https://doi.org/10.1073/pnas.1901642116>
- Ghinassi, M., Billi, P., Libsekal, Y., Papini, M., & Rook, L. (2013). Inferring fluvial morphodynamics and overbank flow control from 3D outcrop sections of a Pleistocene point bar, Dandiero Basin, Eritrea. *Journal of Sedimentary Research*, 83(12), 1065–1083. <https://doi.org/10.2110/jsr.2013.80>
- Gibling, M. R. (2006). Width and thickness of fluvial channel bodies and valley fills in the geological record: A literature compilation and classification. *Journal of Sedimentary Research*, 76(5), 731–770. <https://doi.org/10.2110/jsr.2006.060>
- Gibling, M. R., Davies, N. S., Falcon-Lang, H. J., Bashforth, A. R., DiMichele, W. A., Rygel, M. C., & Ielpi, A. (2014). Palaeozoic co-evolution of rivers and vegetation: A synthesis of current knowledge. *Proceedings of the Geologist's Association*, 125, 524–533. <https://dx.doi.org/10.1016/j.pgeola.2013.12.003>
- Goudge, T. A., Milliken, R. E., Head, J. W., Mustard, J. F., & Fassett, C. I. (2017). Sedimentological evidence for a deltaic origin of the western fan deposit in Jezero crater, Mars and implications for future exploration. *Earth & Planetary Science Letter*, 458, 357–365. <https://doi.org/10.1016/j.epsl.2016.10.056>
- Grabowski, R. C., Droppo, I. G., & Wharton, G. (2011). Erodibility of cohesive sediment: the importance of sediment properties. *Earth-Science Reviews*, 105(3–4), 101–120. <https://doi.org/10.1016/j.earscirev.2011.01.008>
- Graf, W. L. (1978). Fluvial adjustments to the spread of tamarisk in the Colorado Plateau region. *Bulletin of the Geological Society of America*, 89, 1491–1501.
- Gran, K., & Paola, C. (2001). Riparian vegetation controls on braided stream dynamics. *Water Resources Research*, 37(12), 3275–3283. <https://doi.org/10.1029/2000WR002023>
- Grotzinger, J. P., Gupta, S., Malin, M. C., Rubin, D. M., Schieber, J., Siebach, K., et al. (2015). Deposition, exhumation, and paleoclimate of an ancient lake deposit, Gale crater, Mars. *Science*, 350(6257). <https://doi.org/10.1126/science.aac7575>
- Gurnell, A. (2014). Plants as river system engineers. *Earth Surface Processes & Landforms*, 39(1), 4–25. <https://doi.org/10.1002/esp.3397>
- Hartley, A. J., Owen, A., Swan, A., Weissmann, G. S., Holzweber, B. L., Howell, J., et al. (2015). Recognition and importance of amalgamated sandy meander belts in the continental rock record. *Geology*, 43(8), 679–682. <https://doi.org/10.1130/G36743.1>
- Hartley, A. J., Owen, A., Weissman, G. S., & Scuderi, L. (2018). Modern and ancient amalgamated sandy meander-belt deposits: Recognition and controls on development. In M. Ghinassi, L. Colombero, N. Mountney, & A. J. Reesink (Eds.), *Fluvial meanders and their sedimentary products in the rock record, International Associations of Sedimentologists Special Publication* (Vol. 48, pp. 349–384). Malden, MA: Blackwell.
- Hayden, A. T., Lamb, M. P., Fischer, W. W., Ewing, R. C., McElroy, B. J., & Williams, R. M. E. (2019). Formation of sinuous ridges by inversion of river-channel belts in Utah, USA, with implications for Mars. *Icarus*, 332, 92–110. <https://doi.org/10.1016/j.icarus.2019.04.019>
- Hickin, E. J., & Nanson, G. C. (1984). Lateral migration rates of river bends. *Journal of Hydraulic Engineering*, 110, 1557–1567.
- Hinkel, K. M., & Hurd, J. K. Jr. (2006). Permafrost destabilization and thermokarst following snow fence installation, Barrow, Alaska, U.S. *Arctic, Antarctic, & Alpine Research*, 38, 530–539. [https://doi.org/10.1657/1523-0430\(2006\)38\[530:PDATFS\]2.0.CO;2](https://doi.org/10.1657/1523-0430(2006)38[530:PDATFS]2.0.CO;2)

- Howard, A. D., & Knutson, T. R. (1984). Sufficient conditions for river meandering: A simulation approach. *Water Resources Research*, *20*, 1659–1667.
- Huang, H. Q., & Nanson, G. C. (1998). The influence of bank strength on channel geometry: An integrated analysis of some observations. *Earth Surface Processes & Landforms*, *23*, 865–876.
- Ielpi, A. (2018). Morphodynamics of meandering streams devoid of plant life: Amargosa River, Death Valley, California. *Bulletin of the Geological Society of America*, *131*(5-6), 782–802. <https://doi.org/10.1130/B31960.1>
- Ielpi, A., Fralick, P., Ventra, D., Ghinassi, M., Lebeau, L. E., Marconato, A., et al. (2018). Fluvial floodplains prior to greening of the continents: Stratigraphic record, geodynamic settings, and modern analogues. *Sedimentary Geology*, *372*, 140–172. <https://doi.org/10.1016/j.sedgeo.2018.05.009>
- Ielpi, A., & Lapôte, M. G. A. (2019a). Biotic forcing militates against river meandering in the modern Bonneville Basin of Utah. *Sedimentology*, *66*(5), 1896–1929. <https://doi.org/10.1111/sed.12562>
- Ielpi, A., & Lapôte, M. G. A. (2019b). Barren meandering streams in the modern Toiyabe basin of Nevada, and their relevance to the study of the pre-vegetation rock record. *Journal of Sedimentary Research*, *89*(5), 399–415. <https://doi.org/10.2110/jsr.2019.25>
- Ielpi, A., & Rainbird, R. H. (2015). Architecture and morphodynamics of a 1.6 Ga fluvial sandstone: Ellice Formation of Elu Basin, Arctic Canada. *Sedimentology*, *62*(7), 1950–1977. <https://doi.org/10.1111/sed.12211>
- Ielpi, A., & Rainbird, R. H. (2016). Reappraisal of Precambrian sheet-braided rivers: Evidence for 1.9 Ga deep-channelled drainage. *Sedimentology*, *63*(6), 1550–1581. <https://doi.org/10.1111/sed.12273>
- Ielpi, A., Rainbird, R. H., Ventra, D., & Ghinassi, M. (2017). Morphometric convergence between Proterozoic and post-vegetation rivers. *Nature Communications*, *8*. <https://doi.org/10.1038/ncomms15252>
- Ielpi, A., Ventra, D., & Ghinassi, M. (2016). Deeply channelled Precambrian rivers: Remote sensing and outcrop evidence from the 1.2 Ga Stoer Group of NW Scotland. *Precambrian Research*, *281*, 291–311. <https://doi.org/10.1016/j.precamres.2016.06.004>
- Ikeda, S., Parker, G., & Sawai, K. (1981). Bend theory of river meanders. Part 1. Linear development. *Journal of Fluid Mechanics*, *112*, 363–377.
- Jackson, R. G. II (1975). Velocity–bed-form–texture patterns of meander bends in the lower Wabash River of Illinois and Indiana. *Bulletin of the Geological Society of America*, *86*, 1511–1522.
- Jackson, R. G. II (1976). Depositional model of point bars in the Lower Wabash River. *Journal of Sedimentary Petrology*, *46*(3), 579–594.
- Jacobsen, R. E., & Burr, D. M. (2016). Greater contrast in Martian hydrological history from more accurate estimates of paleodischarge. *Geophysical Research Letters*, *43*, 8903–8911. <https://doi.org/10.1002/2016GL070535>
- Jacobsen, R. E., & Burr, D. M. (2018). Errors in Martian paleodischarges skew interpretations of hydrologic history: Case study of the Aeolis Dorsa, Mars, with insights from the Quinn River, NV. *Icarus*, *302*, 407–417. <https://doi.org/10.1016/j.icarus.2017.11.014>
- Kean, J. W., Kuhnle, R. A., Smith, J. D., Alonso, C. V., & Langendoen, E. J. (2009). Test of a method to calculate near-bank velocity and boundary shear stress. *Journal of Hydraulic Engineering*, *135*(7), 588–601. [https://doi.org/10.1061/\(ASCE\)HY.1943-7900.0000049](https://doi.org/10.1061/(ASCE)HY.1943-7900.0000049)
- Kean, J. W., & Smith, J. D. (2004). Flow and boundary shear stress in channels with woody bank vegetation. In S. J. Bennett & A. Simon (Eds.), *Riparian vegetation and fluvial geomorphology*, AGU Water Science Application Series (Vol. 8, pp. 237–252). Washington, DC: American Geophysical Union.
- Kite, E. S., Howard, A. D., Lucas, A., & Lewis, K. W. (2015). Resolving the era of river-forming climates on Mars using stratigraphic logs of river-deposit dimensions. *Earth & Planetary Science Letters*, *420*, 55–65. <https://doi.org/10.1016/j.epsl.2015.03.019>
- Kleinhans, M. G., Braudrick, C., van Dijk, W. M., van de Lageweg, W. I., Teske, R., & van Oorschot, M. (2015). Swiftiness of bio-morphodynamics in Lilliput- to Giant-sized rivers and deltas. *Geomorphology*, *244*, 56–73. <https://doi.org/10.1016/j.geomorph.2015.04.022>
- Kleinhans, M. G., van Dijk, W. M., van de Lageweg, W. I., Hoyal, D. C. J. D., Markies, H., van Maarseveen, M., et al. (2014). Quantifiable effectiveness of experimental scaling of river- and delta morphodynamics and stratigraphy. *Earth-Science Reviews*, *133*, 43–61. <https://doi.org/10.1016/j.earscirev.2014.03.001>
- Knight, D. W., Demetriou, J. D., & Hamed, M. E. (1984). Boundary shear in smooth rectangular channels. *Journal of Hydraulic Engineering*, *110*, 405–422.
- Konsoer, K. M., LeRoy, J., Burr, D., Parker, G., Jacobsen, R., & Turmel, D. (2018). Channel slope adjustment in reduced gravity environments and implications for Martian channels. *Geology*, *46*(2), 183–186. <https://doi.org/10.1130/G39666.1>
- Lapôte, M. G. A., Lamb, M. P., & McElroy, B. (2017). What sets the size of current ripples? *Geology*, *45*(3), 243–246. <https://doi.org/10.1130/G38598.1>
- Lawler, D. (1986). River bank erosion and the influence of frost: A statistical examination. *Transactions of the Institute of British Geographers*, *11*(2), 227–242.
- Leopold, L. B., & Wolman, M. G. (1960). River meanders. *Bulletin of Geological Society of America*, *71*, 769–793.
- Li, C., Czupiga, M. J., Eke, E. C., Viparello, E., & Parker, G. (2015). Variable Shields number model for river bankfull geometry: Bankfull shear velocity is viscosity-dependent but grain size-independent. *Journal of Hydraulic Research*, *53*(1), 36–48. <https://doi.org/10.1080/00221686.2014.939113>
- Limaye, A. B., Grimaud, J. L., Lai, S. Y., Foreman, B. Z., Komatsu, Y., & Paola, C. (2018). Geometry and dynamics of braided channels and bars under experimental density currents. *Sedimentology*, *65*, 1947–1972. <https://doi.org/10.1111/sed.12453>
- Limaye, A. B., & Lamb, M. P. (2013). A vector-based method for bank-material tracking in coupled models of meandering and landscape evolution. *Journal of Geophysical Research: Earth Surface*, *118*, 2421–2437. <https://doi.org/10.1002/2013JF002854>
- Long, D. G. F. (1978). Proterozoic stream deposits: Some problems of recognition and interpretation of ancient sandy fluvial systems. In A. D. Miall (Ed.), *Fluvial sedimentology* (Vol. 5, pp. 313–342). Calgary, Canada: Canadian Society of Petroleum Geology.
- Long, D. G. F. (2011). Architecture and depositional style of fluvial systems before land plants: A comparison of Precambrian, early Paleozoic, and modern river deposits. In S. K. Davidson, S. Leleu, & C. P. North (Eds.), *From river to rock record: The preservation of fluvial sediments and their subsequent interpretation* (Vol. 97, pp. 37–61). Tulsa, OK: SEPM.
- Lynds, R. M., Mohrig, D., Hajek, E. A., & Heller, P. L. (2014). Paleoslope reconstruction in sandy suspended-load-dominant rivers. *Journal of Sedimentary Research*, *84*(10), 825–836. <https://doi.org/10.2110/jsr.2014.60>
- Mahon, R. C., & McElroy, B. (2018). Indirect estimation of bedload flux from modern sand-bed rivers and ancient fluvial strata. *Geology*, *46*(7), 579–582. <https://doi.org/10.1130/G4016.11>
- Matsubara, Y., & Howard, A. D. (2014). Modeling planform evolution of a mud-dominated meandering river: Quinn River, Nevada, USA. *Earth Surface Processes & Landforms*, *39*(10), 1365–1377. <https://doi.org/10.1002/esp.3588>

- Matsubara, Y., Howard, A. D., Burr, D. M., Williams, R. M., Dietrich, W. E., & Moore, J. M. (2015). River meandering on Earth and Mars: A comparative study of Aeolis Dorsa meanders, Mars and possible terrestrial analogs of the Usuktuk River, AK, and the Quinn River, NV. *Geomorphology*, *240*, 102–120. <https://doi.org/10.1016/j.geomorph.2014.08.031>
- McLelland, S. J., Ashworth, P. J., Best, J. L., Roden, J., & Klaassen, G. J. (1999). Flow structure and transport of sand-grade suspended sediment around an evolving braid bar, Jamuna River, Bangladesh. In N. D. Smith & J. Rogers (Eds.), *Fluvial sedimentology VI, International Associations of Sedimentologists Special Publication* (Vol. 28, pp. 43–57). Malden, MA: Blackwell.
- McLennan, S. M., Grotzinger, J. P., Hurowitz, J. A., & Tosca, N. J. (2019). The sedimentary cycle on Early Mars. *Annual Reviews of Earth & Planetary Sciences*, *47*, 91–118. <https://doi.org/10.1146/annurev-earth-053018-060332>
- McMahon, W. J., & Davies, N. S. (2018a). Evolution of alluvial mudrock forced by early land plants. *Science*, *359*(6379), 1022–1024. <https://doi.org/10.1126/science.aan4660>
- McMahon, W. J., & Davies, N. S. (2018b). The shortage of geological evidence for pre-vegetation meandering rivers. In M. Ghinassi, L. Colombero, N. Mountney, & A. J. Reesink (Eds.), *Fluvial meanders and their sedimentary products in the rock record, International Associations of Sedimentologists Special Publication* (Vol. 48, pp. 119–148). Malden, MA: Blackwell.
- Métivier, F., Lajeunesse, E., & Devauchelle, O. (2017). Laboratory rivers: Lacey's law, threshold theory, and channel stability. *Earth Surface Dynamics*, *5*, 187–198. <https://doi.org/10.5194/esurf-5-187-2017>
- Micheli, E. R., & Kirchner, J. W. (2002). Effects of wet meadow riparian vegetation on streambank erosion. 2. Measurements of vegetated bank strength and consequences for failure mechanics. *Earth Surface Processes & Landforms*, *27*(7), 687–697. <https://doi.org/10.1002/esp.340>
- Micheli, E. R., Kirchner, J. W., & Larsen, E. W. (2004). Quantifying the effect of riparian forest versus agricultural vegetation on river meander migration rates, Central Sacramento River, California, USA. *River Research & Applications*, *20*(5), 537–548. <https://doi.org/10.1002/rra.756>
- Mitchener, H., & Torfs, H. (1996). Erosion of mud/sand mixtures. *Coastal Engineering*, *29*(1-2), 1–25.
- Millar, R. G. (2000). Influence of bank vegetation on alluvial channel patterns. *Water Resources Research*, *36*(4), 1109–1118. <https://doi.org/10.1029/1999WR900346>
- Millar, R. G., & Quick, M. C. (1993). Effect of bank stability on geometry of gravel rivers. *Journal of Hydraulics Engineering*, *119*, 1343–1363.
- Millar, R. G., & Quick, M. C. (1998). Stable width and depth of gravel-bed rivers with cohesive banks. *Journal of Hydraulic Engineering*, *124*, 1005–1013.
- Mohrig, D., Heller, P. L., Paola, C., & Lyons, W. J. (2000). Interpreting avulsion process from ancient alluvial sequences: Guadalupe-Matarranya system (northern Spain) and Wasatch Formation (western Colorado). *Bulletin of the Geological Society of America*, *112*(12), 1787–1803. [https://doi.org/10.1130/0016-7606\(2000\)112<1787:IAPFAA>2.0.CO;2](https://doi.org/10.1130/0016-7606(2000)112<1787:IAPFAA>2.0.CO;2)
- Moreton, D. J., Ashworth, P., & Best, J. L. (2002). The physical scale modelling of braided alluvial architecture and estimation of subsurface permeability. *Basin Research*, *14*(3), 265–285. <https://doi.org/10.1046/j.1365-2117.2002.00189.x>
- Mukhopadhyay, S., Choudhuri, A., Samanta, P., Sarkar, S., & Bose, P. K. (2014). Were the hydraulic parameters of Precambrian rivers different? *Journal of Asian Earth Sciences*, *91*, 289–297. <https://doi.org/10.1016/j.jseas.2013.07.042>
- Murray, A. B., & Paola, C. (2003). Modelling the effect of vegetation on channel pattern in bedload rivers. *Earth Surface Processes & Landforms*, *28*(2), 131–143. <https://doi.org/10.1002/esp.428>
- Mustard, J. F., Murchie, S. L., Pelkey, S. M., Ehlmann, B. L., Milliken, R. E., Grant, J. A., et al. (2008). Hydrated silicate minerals on Mars observed by the Mars Reconnaissance Orbiter CRISM instrument. *Nature*, *454*, 305–309. <https://doi.org/10.1038/nature07097>
- Nelson, P. A., & Seminara, G. (2011). Modeling the evolution of bedrock channel shape with erosion from saltating bed load. *Geophysical Research Letters*, *38*, L17406. <https://doi.org/10.1029/2011GL048628>
- Nichols, G. (2012). Endorheic basins. In C. Busby & A. Azor (Eds.), *Tectonics of sedimentary basins: Recent advances* (pp. 621–632). Chichester, UK: Blackwell.
- Niño, Y., Lopez, F., & Garcia, M. (2003). Threshold for particle entrainment into suspension. *Sedimentology*, *50*(2), 247–263. <https://doi.org/10.1046/j.1365-3091.2003.00551.x>
- Parker, G. (1976). On the cause and characteristic scales of meandering and braiding in rivers. *Journal of Fluid Mechanics*, *76*, 457–480.
- Parker, G. (1978). Self-formed straight rivers with equilibrium banks and mobile bed. Part 2. The gravel river. *Journal of Fluid Mechanics*, *89*, 127–146.
- Parker, G., Shimizu, Y., Wilkerson, G. V., Eke, E. C., Abad, J. D., Lauer, J. W., et al. (2011). A new framework for modeling the migration of meandering rivers. *Earth Surface Processes & Landforms*, *36*(1), 70–86. <https://doi.org/10.1002/esp.2113>
- Parker, G., Wilcock, P. R., Paola, C., Dietrich, W. E., & Pitlick, J. (2007). Physical basis for quasi-universal relations describing bankfull hydraulic geometry of single-thread gravel bed rivers. *Journal of Geophysical Research*, *112*(F4). <https://doi.org/10.1029/2006JF000549>
- Peakall, J., Ashworth, P. J., & Best, J. L. (2007). Meander-bend evolution, alluvial architecture, and the role of cohesion in sinuous river channels: a flume study. *Journal of Sedimentary Research*, *77*(3), 197–212. <https://doi.org/10.2110/jsr.2007.017>
- Polvi, L. E., Wohl, E., & Merritt, D. M. (2014). Modeling the functional influence of vegetation type on streambank cohesion. *Earth Surface Processes & Landforms*, *39*(9), 1245–1258. <https://doi.org/10.1002/esp.3577>
- Poulet, F., Bibring, J.-P., Mustard, J. F., Gendrin, A., Mangold, N., Langevin, Y., et al., & the OMEGA Team (2005). Phyllosilicates on Mars and implications for early Martian climate. *Nature*, *438*, 623–627. <https://doi.org/10.1038/nature04274>
- Santos, M. G. M., Hartley, A. J., Mountney, N. P., Peakall, J., Owen, A., Merino, E. R., & Assine, M. L. (2019). Meandering rivers in modern desert basins: Implications for channel planform controls and prevegetation rivers. *Sedimentary Geology*, *385*, 1–14. <https://doi.org/10.1016/j.sedgeo.2019.03.011>
- Santos, M. G. M., & Owen, G. (2016). Heterolithic meandering-channel deposits from the Neoproterozoic of NW Scotland: Implications for palaeogeographic reconstructions of Precambrian sedimentary environments. *Precambrian Research*, *272*, 226–243. <https://doi.org/10.1016/j.precamres.2015.11.003>
- Schieber, J., Bish, D., Coleman, M., Reed, M., Hausrath, E.M., Cosgrove, J., et al. (2017). Encounters with an unearthy mudstone: Understanding the first mudstone found on Mars. *Sedimentology*, *64*(2), 311–358. <https://doi.org/10.1111/sed.12318>
- Schon, S. C., Head, J. W., & Fassett, C. I. (2012). An overfilled lacustrine system and progradational delta in Jezero crater, Mars: Implications for Noachian climate. *Planetary & Space Science*, *67*(1), 28–45. <https://doi.org/10.1016/j.pss.2012.02.003>
- Schumm, S. A. (1960). The shape of alluvial channels in relation to sediment type. *United States Geological Survey Professional Paper*, *352*, 17–30.
- Schumm, S. A. (1963). Sinuosity of alluvial rivers on the Great Plains. *Bulletin of the Geological Society of America*, *74*, 1089–1100.

- Schumm, S. A. (1968). Speculations concerning paleohydrologic controls of terrestrial sedimentation. *Bulletin of the Geological Society of America*, 79, 1573–1588.
- Scott, K. M. (1978). Effects of permafrost on stream channel behavior in arctic Alaska. *United States Geological Survey Professional Paper*, 1068, 1–19.
- Seminara, G., & Tubino, M. (1989). Alternate bar and meandering: Free, forced, and mixed interactions. In S. Ikeda & G. Parker (Eds.), *River meandering, water research monographs* (Vol. 12, pp. 267–320). Washington, DC: American Geophysical Union.
- Simon, A., & Collison, A. J. C. (2002). Quantifying the mechanical and hydrologic effects of riparian vegetation on streambank stability. *Earth Surface Processes & Landforms*, 27(5), 527–546. <https://doi.org/10.1002/esp.325>
- Smith, D. G. (1976). Effect of vegetation on lateral migration of anastomosed channels of a glacier meltwater river. *Bulletin of the Geological Society of America*, 87, 857–860.
- Smith, N. D., & Smith, D. G. (1984). William River: An outstanding example of channel widening and braiding caused by bed-load addition. *Geology*, 12, 78–82.
- Soulsby, R., & Whitehouse, R. (1997). Threshold of sediment motion in coastal environments. In *Pacific Coasts and Ports '97: Proceedings of the 13th Australasian Coastal & Ocean Engineering Conference and the 6th Australasian Port and Harbor Conference* (Vol. 1, pp. 145–150). Christchurch, New Zealand: Center for Advanced Engineering, University of Canterbury.
- Struikma, N., Olesen, K., Flokstra, D., & De Vriend, H. (1985). Bed deformation in curved alluvial channels. *Journal of Hydraulic Research*, 23(1), 57–79.
- Swan, A., Hartley, A. J., Owen, A., & Howell, J. (2018). Reconstruction of a sandy point-bar deposit: Implications for fluvial facies analysis. In M. Ghinassi, L. Colombera, N. Mountney, & A. J. Reesink (Eds.), *Fluvial meanders and their sedimentary products in the rock record, International Associations of Sedimentologists Special Publication* (Vol. 48, pp. 445–474). Malden, MA: Blackwell.
- Sylvester, Z., Durkin, P., & Covault, J. A. (2019). High curvatures drive river meandering. *Geology*, 47(3). <https://doi.org/10.1130/G45608.1>
- Takagi, T., Oguchi, T., Matsumoto, J., Grossman, M. J., Sarker, M. H., & Matin, M. A. (2007). Channel braiding and stability of the Brahmaputra River, Bangladesh, since 1967: GIS and remote sensing analyses. *Geomorphology*, 85(3–4), 294–305. <https://doi.org/10.1016/j.geomorph.2006.03.028>
- Tal, M., & Paola, C. (2007). Dynamic single-thread channels maintained by the interaction of flow and vegetation. *Geology*, 35, 347–350. <https://doi.org/10.1130/G23260A.1>
- Ternat, F., Boyer, P., Anselmet, F., & Amielh, M. (2008). Erosion threshold of saturated natural cohesive sediments: Modeling and experiments. *Water Resources Research*, 44, W11434. <https://doi.org/10.1029/2007WR006537>
- Tosca, N. J., Johnston, D. T., Mushegian, A., Rothman, D. H., Summons, R. E., & Knoll, A. H. (2010). Clay mineralogy, organic carbon burial, and redox evolution in Proterozoic oceans. *Geochimica et Cosmochimica Acta*, 74(5), 1579–1592. <https://doi.org/10.1016/j.gca.2009.12.001>
- Trampush, S., Huzurbazar, S., & McElroy, B. (2014). Empirical assessment of theory for bankfull characteristics of alluvial channels. *Water Resources Research*, 50, 9211–9220. <https://doi.org/10.1002/2014WR015597>
- van Dijk, W., van de Lageweg, W. I., & Kleinhans, M. G. (2012). Experimental meandering river with chute cutoffs. *Journal of Geophysical Research*, 117(F3). <https://doi.org/10.1029/2011JF002314>
- van Dijk, W., van de Lageweg, W. I., & Kleinhans, M. G. (2013). Formation of a cohesive floodplain in a dynamic experimental meandering river. *Earth Surface Processes & Landforms*, 38(13), 1550–1565. <https://doi.org/10.1002/esp.3400>
- Wilkerson, G. V., & Parker, G. (2010). Physical basis for quasi-universal relationships describing bankfull hydraulic geometry of sand-bed rivers. *Journal of Hydraulic Engineering*, 137, 739–753. [https://doi.org/10.1061/\(ASCE\)HY.1943-7900.0000352](https://doi.org/10.1061/(ASCE)HY.1943-7900.0000352)
- Williams, G. P. (1986). River meanders and channel size. *Journal of Hydrology*, 88, 147–164.
- Williams, R. M., Irwin, R. P. III, Burr, D. M., Harrison, T., & McClelland, P. (2013). Variability in Martian sinuous ridge form: Case study of Aeolis Serpens in the Aeolis Dorsa, Mars, and insight from the Mirackina paleoriver, South Australia. *Icarus*, 225(1), 308–324. <https://doi.org/10.1016/j.icarus.2013.03.016>
- Wolman, M. G. (1959). Factors influencing erosion of a cohesive river bank. *American Journal of Science*, 257, 204–216.
- Wright, S., & Parker, G. (2004). Flow resistance and suspended load in sand-bed rivers: Simplified stratification model. *Journal of Hydraulic Engineering*, 130, 769–805. [https://doi.org/10.1061/\(ASCE\)0733-9429\(2004\)130:5\(796\)](https://doi.org/10.1061/(ASCE)0733-9429(2004)130:5(796))